UNIVERSIDADE DE LISBOA
FACULDADE DE CIÊNCIAS
DEPARTAMENTO DE BIOLOGIA VEGETAL

NLRP3 inflammasome-driven neurodegeneration and epileptiform activity in a model of epileptogenesis in organotypic slices

Francisco José Gonçalves Meda

Mestrado em Biologia Molecular e Genética

Dissertação orientada por:
Doutora Cláudia Alexandra dos Santos Valente de Castro
Doutor Federico Herrera Garcia

2020

Acknowledgements

Neste atípico ano, caracterizado pelo afastamento social, tive a oportunidade de conhecer e me aproximar de várias pessoas, nomeadamente durante a minha passagem pelo laboratório da Prof. Ana Sebastião, à qual desde já agradeço pela oportunidade dada de me inserir num dos seus projetos.

À minha orientadora Cláudia, gostaria de agradecer por me ter aceite como seu aluno e pela disponibilidade demonstrada, mesmo quando não estava presente, estando sempre ao alcance de uma simples chamada. Além disso, agradeço o esforço e dedicação para com o trabalho que desenvolvi este passado ano.

A todos os membros do laboratório ASebastião pela simpatia e disponibilidade para ajudar em qualquer situação, o que fez com que me integrasse muito melhor no mesmo. Dentro destes queria agradecer em especial à Leonor Rodrigues por me transmitir os conhecimentos de eletrofisiologia e aos Valentes! Aqueles que me acompanharam praticamente todos os dias no trabalho de bancada, a Mafalda, a Mariana e o Diogo, ajudando não só em momentos de trabalho, mas também contribuindo para momentos de brincadeira e descontração.

A todos os meus amigos, que apesar de longe conseguem estar sempre perto.

Aos meus pais, por sempre se esforçarem para que não me falte nada, respeitando e apoiando todas as minhas escolhas.

Tudo isto contribui para que este ano corresse da melhor forma possível, quer pessoal, quer profissionalmente.

Resumo

A epilepsia é uma doença neurológica que afeta mundialmente cerca de 65 milhões de pessoas, tornando-a uma das mais comuns em todo o mundo. Esta doença é caracterizada pela predisposição para gerar convulsões periódicas e imprevisíveis, isto é, episódios de atividade neuronal sincronizada e excessiva. Apesar da existência de fármacos antiepiléticos, um terço dos pacientes continuam a sofrer progressão da doença e declínio cognitivo, tornando imperativo o desenvolvimento de novas estratégias terapêuticas, tentando assim prevenir ou atrasar as consequências da epilepsia.

Vários estudos demonstram que a epilepsia está fortemente associada à neuroinflamação. A epilepsia do lobo temporal, uma das formas mais comuns e severas de epilepsia, ataca maioritariamente o hipocampo e está relacionada com eventos inflamatórios que culminam em morte neuronal e aumento de expressão de fatores inflamatórios. Um dos principais fatores é a interleucina-1β (IL-1β), que promove disfunção sináptica, hiperexcitabilidade e morte neuronal. Em circunstâncias fisiológicas, a neuroinflamação tem efeitos benéficos, atuando como proteção contra infeções e reparação de danos, mas quando a sua duração e intensidade excedem o limite homeostático, pode tornar-se crónica e ter efeitos severos como a indução de doenças do foro neurológico, tais como a Doença de Alzheimer ou a epilepsia. Visto isto, a neuroinflamação é considerada como um potencial alvo terapêutico para o combate à epilepsia.

Recentemente, o inflamassoma NLRP3 tem sido frequentemente associado ao processo de epileptogénese. Este complexo multiproteico citoplasmático é constituído por 3 componentes, um sensor (NLRP3), um adaptador (ASC) e um efetor (Caspase-1), sendo responsável pela maturação da IL-1β por ativação da Caspase-1 e é considerado um fator-chave para a propagação e regulação da neuroinflamação. Este inflamassoma tem sido associado à morte celular por piroptose, um processo mediado pela Gasdermin D (GSDMD) quando clivada pela Caspase-1, no contexto de várias doenças neurológicas. A morte neuronal é uma das principais características da epilepsia, mas a relevância da morte neuronal por piroptose não está ainda esclarecida nesta patologia. Estudos demonstram que a inibição do NLRP3, tem um efeito neuroprotetor num modelo animal de epilepsia. Resultados preliminares obtidos no grupo, indicam que o MCC950, um inibidor seletivo deste complexo multiproteico, é capaz de diminuir a atividade epileptiforme de fatias organotípicas.

Este estudo pretende avaliar a progressão da atividade epileptiforme e a ocorrência de morte neuronal por piroptose num modelo de epileptogénese *ex vivo*, assim como explorar a influência do inflamassoma NLRP3 na geração destes eventos. Foi utilizado um modelo de epileptogénese em fatias organotípicas de córtex rinal e hipocampo preparadas a partir de ratos Sprague-Dawley com 6-7 dias de vida (P6-7). Este modelo é uma ferramenta simples e útil no estudo da epileptogénese, já que replica características do ambiente *in vivo* do hipocampo como a conectividade neuronal e a plasticidade sináptica, permitindo assim, a geração de atividade epileptiforme. Além disso, as fatias organotípicas podem ser mantidas por longos períodos de tempo, o que permite a sua manipulação e estudos a longo prazo. Para os ensaios realizados foram recolhidas amostras aos dias 3, 7, 14, e 21 *in vitro* (DIV), permitindo assim o estudo da evolução, não só da atividade epileptiforme, bem como da morte neuronal e presença do inflamassoma em neurónios.

A atividade epileptiforme foi avaliada através de registos eletrofisiológicos, obtidos numa câmara de interface. A atividade foi captada por registos eletrofisiológicos na região da cornus ammonis 3 (CA3), já que é a mais frequentemente afetada por *bursts* de atividade ictal. Este tipo de atividade é caracterizada por surtos contínuos de eventos epiléticos que duram mais de 10s e distinguidos entre si quando o intervalo que os separa é maior que 2s. O efeito do MCC950 na atividade epileptiforme também foi avaliado através de registos eletrofisiológicos. A morte celular foi avaliada pela incorporação celular de

iodeto de propídio (PI). Este composto fluorescente incorpora-se entre os ácidos nucleicos de células com membrana permeabilizada, permitindo assim distinguir células em processo de morte celular. Também o progresso da expressão da proteína efectora da piroptose (GSDMD) e dos componentes do inflamassoma NLRP3, foram avaliados por western blot, e por ensaios de imunohistoquímica paralelamente a um marcador nuclear de neurónios (NeuN). A produção de espécies reativas de oxigénio (ROS), potenciais ativadores do inflamassoma no sistema em estudo, foi avaliada usando um composto que após ser clivado por ROS, gera um produto fluorescente que pode ser detetado por microscopia de fluorescência.

A atividade epileptiforme foi caracterizada pelos seguintes parâmetros: número e duração de *bursts*, número de eventos por *burst*, amplitude e frequência. A maioria dos parâmetros atinge o máximo em fatias com 13-15 DIV, onde a atividade epileptiforme é maioritariamente ictal. Os valores de IL-1β libertada estão de acordo com o climax de atividade detetada, já que aumentam progressivamente até atingirem o máximo ao 17 DIV. O ensaio de morte celular revelou desigualdades entre as zonas do hipocampo, sendo os neurónios granulares do giro denteado (DG) e os neurónios piramidais da CA1 mais afetados que os neurónios da CA3, o que vai de acordo com a literatura. Em relação à progressão da morte celular, além da CA3 que demonstra decréscimo significativo de 7 a 21 DIV, as restantes regiões não apresentam alterações consideráveis, provavelmente devido ao baixo número de fatias avaliadas. É de notar que todas as zonas mostraram elevada incidência de morte neuronal ao 3 DIV, o que pode ser explicado pelo stress causado pelo corte das fatias. A clivagem de GSDMD no hipocampo mostra máximos ao 7 DIV reduzindo até ao final da cultura. Para além disso, ocorre co-localização de GSDMD com neurónios, confirmando morte neuronal por piroptose no modelo de epileptogénese em estudo. Resultados anteriores referentes à αII-Espetrina, que quando clivada por protéases associadas a processos de morte neuronal, nomeadamente calpaínas, origina produtos intervenientes no processo de morte por necrose, indicam morte neuronal por necrose a tempos mais tardios de cultura. Estes resultados sugerem prevalência de morte neuronal por piroptose até ao 7 DIV, mas ao longo do tempo em cultura, a necrose passa a ser a forma principal de morte neuronal.

A expressão dos componentes do inflamassoma foi avaliada neste sistema ao longo do tempo de cultura. A diminuição do domínio NLRP3 é explicada pela ausência de estímulos de *priming* no sistema, não sendo portanto estimulada a sua expressão. Quanto ao ASC e à Caspase-1, não são verificadas diferenças significativas, mas a expressão da Caspase-1 demonstra uma tendência para aumento de 3 para 7 DIV, sugerindo ativação do inflamassoma. Os ensaios de imunohistoquímica detetaram componentes do inflamassoma, nomeadamente o NLRP3 e o ASC, em neurónios, o que contribui com mais provas de que o complexo está presente em neurónios, facto ainda pouco descrito pela comunidade científica. Apesar da expressão do inflamassoma diminuir ao longo do tempo de cultura, os resultados sugerem a sua ativação por ROS, já que os valores de ROS aumentam com o tempo em cultura, especialmente em DG e CA1, onde efetivamente ocorre prevalência de morte neuronal.

A ação inibitória do MCC950 sobre o NLRP3 teve um impacto evidente na atividade epileptiforme. A sua presença durante os registos electrofisiológicos quase anulou a atividade ictal, com uma diminuição significativa em praticamente todos os parâmetros avaliados. Isto demonstra que o NLRP3 está diretamente envolvido na geração da atividade epileptiforme no sistema em estudo.

Em suma, este trabalho demonstrou ocorrência de morte neuronal por piroptose mediada pelo inflamassoma NLRP3. Igualmente provou que a inibição deste complexo consegue reduzir significativamente a geração de atividade epileptiforme espontânea, podendo assim ser um potential alvo terapêutico para a epilepsia.

Palavras-Chave: Epilepsia, atividade epileptiforme, inflamassoma NLRP3, piroptose, MCC950.

Abstract

Epilepsy is a neurological disorder characterized by periods of spontaneous and excessive brain activity. It affects 65 million people worldwide, and despite the available therapies, 30-40% of the patients keep suffering from epilepsy and cognitive regress.

Studies showed a correlation between epilepsy and neuroinflammatory events, and neuroinflammation is nowadays considered a potential therapeutic target for this pathology. NOD-, LRR- and pyrin domain-containing protein 3 (NLRP3) inflammasome, a cytoplasmic multiproteic complex composed by a sensor (NLRP3), an adaptor (ASC) and an effector (Caspase-1), has been implicated in a wide range of neurological diseases. This complex initiates pyroptosis, an inflammatory type of cell death, through Gasdermin D (GSDMD) cleavage by Caspase-1 and subsequent release of Interleukin-1β (IL-1β). Neuronal death is one of the hallmarks of epilepsy, but neuronal death by pyroptosis is still unexplored in this context.

Previous results have shown, that NLRP3 inflammasome inhibition has a neuroprotective effect in an animal model of epilepsy. Furthermore, preliminary results indicate that MCC950, a selective inhibitor of this complex, can decrease the epileptiform activity of organotypic slices.

In this project, we aimed to assess the occurrence of neuronal death by pyroptosis in a context of epilepsy and evaluate the impact of NLRP3 inflammasome inhibition upon epileptiform activity. This work was performed in a model of epileptogenesis in rhinal-cortex hippocampus organotypic slices, a model that resembles *in vivo* epilepsy and allows the recording of epileptiform activity, as it maintains neuronal interactions and the characteristics of epilepsy.

This work used rhinal-cortex hippocampus organotypic slices obtained from Sprague-Dawley rats with 6 to 7 days. Epileptiform activity was characterized through several parameters, showing peak activity between 13-15 DIV slices, with overwhelming ictal discharges. Also, interleukin 1β (IL-1β) released, increases until a peak is reached at 17 DIV. Regarding cellular death, slices showed increased PI uptake in the DG and CA3 cell layers, with substantial GSDMD expression in granular and pyramidal neurons, reducing to 21 DIV. In the hippocampus, the expression of NLRP3 domain decreases until 21 DIV, while ASC and Caspase-1 show no significant differences. Presence of NLRP3 and ASC in granular and pyramidal neurons, as well as increased ROS production in these areas, was confirmed, suggesting NLRP3 activation by ROS and NLRP3-mediated neuronal death by pyroptosis in the hippocampus. Additionally, MCC950, almost nullified overwhelming ictal-like epileptiform activity, with the decline of all parameters assessed.

Overall, this study showed the occurrence of neuronal death by pyroptosis mediated by NLRP3 inflammasome. Furthermore, the inhibition of this complex significantly halts the progression of ictal-like activity, thus being a potential therapeutic target for epilepsy.

Keywords: Epilepsy, epileptiform activity, NLRP3 inflammasome, pyroptosis, MCC950.

Index

List of Abbreviations

AD	Alzheimer's Disease
AED	Anti-epileptic drugs
ALR	AIM2-like-receptor
ANOVA	Analysis of Variance
ASC	Apoptosis-associated speck-like protein containing a CARD
AST	Carotenoid astaxanthin
ATP	Adenosine triphosphate
BBB	Blood brain barrier
BIR	Baculoviral inhibitory repeat
BRCC3	JAMM domain containing Zn2+ metalloprotease
BSA	Bovine serum albumin
CA1	Cornus ammonis 1
CA3	Cornus ammonis 3
CAPS	Cryopyrin-associated periodic syndromes
CARD	Caspase activation and recruitment domain
CNS	Central nervous system
CRID	Cytokine release inhibitory drugs
CTL	C-type lectin receptors
DAMP	Damage associated molecular pattern
DCFDA	2,7-dichlorofluorescin diacetate
DG	Dentate gyrus
DIV	*Days in vitro*
DMSO	Dimethyl sulfoxide
EL	Epileptic-like
FCAS	Familial cold autoinflammatory syndrome
GAPDH	Glyceraldehyde 3-phosphate dehydrogenase
GBSS	Gey's balanced salt solution
GSDMD	Gasdermin D
HMGB1	High mobility group box 1
HRP	Horseradish peroxidase
HS	Horse serum

IL-1β	Interleukin-1β
LeTx	*Bacillus anthracis* lethal toxin
LPS	Lipopolysaccharide
MAPK	Mitogen-activated protein kinases
MDP	Bacterial muramyl dipeptide
MPC	Multi protein complex
MS	Multiple sclerosis
MTLE	Medial temporal lobe epilepsy
MWS	Muckle-Wells syndrome
NATCH	Nucleotide-binding and oligomerization domain
NBA	Neurobasal-A medium
Nek7	Serine/threonine protein kinase
NF-kB	Neuronal factor kB
NLR	Nucleotide binding domain and leucine rich repeat
NLRP3	NATCH, LRR and PYD domains-containing protein 3
NMDA	N-methyl-D-aspartate
NR2B	NMDA receptor subunit 2B
OHSC	Organotypic hippocampal slice cultures
P2X7	P2X purinergic receptor 7
PAMP	Pathogen associated molecular pattern
PBS	Phosphate saline buffer
PD	Parkinson’s Disease
PI	Propidium iodide
PRR	Pattern recognition receptor
PVDF	Polyvinylidene fluoride
PYD	Pyrin domain
RA	Rheumatoid arthritis
RLR	RIG-I-like proteins
ROS	Reactive oxygen species
RT	Room temperature
SAE	Sepsis-associated encephalopathy
SBPD	Spectrin breakdown products

SDS	Sodium dodecyl sulphate
SE	*Status epilepticus*
SEM	Standard error of the mean
TBI	Traumatic brain injury
TLR	Toll-like receptors
TNF-α	Tumor necrosis factor α
TWIK2	Two-pore domain weak inwardly rectifying K+ channel 2

List of Figures

1. Introduction

1.1. Epilepsy

Epilepsy, one of the most common neurologic diseases worldwide, is defined by an enduring predisposition to generate synchronized and excessive epileptic seizures. At the cellular level, this pathology is characterized by synchronous and paroxysmal depolarisations, which cause neuronal populations to fire bursts of action potentials. Despite the numerous antiepileptic drugs (AEDs) available, one-third of patients are still refractory to therapy, continue to experience seizures, and suffer progression of the disease, with increasing seizure frequency and cognitive decline.

Commonly, epilepsy requires the occurrence of at least one seizure, however, the official terminology according to The International League Against Epilepsy includes the occurrence of at least two unprovoked seizures >24h apart, one unprovoked seizure with probability of recurrence (at least 60%) and the diagnosis of an epileptic syndrome, defined by seizure types, electroencephalogram patterns and age of onset [1,2]. After diagnosis, the etiology of the disease (genetic, infectious, metabolic, immune or unknown) is key to determine the treatment path to follow [2].

Whilst in most neurodegenerative diseases, such as Alzheimer's disease (AD) and Parkinson's disease (PD), age of onset is a key factor as they affect mainly elderly individuals, epilepsy is known to affect both sexes and all ages [3,4]. However, despite the disease distribution between all ages, aging is still a risk factor, as for most central nervous system (CNS) related diseases [5,6]. Epilepsy incidence is rising due to higher prevalence in developing countries, disregarding age, due to inadequate health care. Also, as science and medicine keep evolving, diagnosis tools are becoming better and better and, as such, more cases are being uncovered, increasing even further the incidence of this disease [3,7,8].

1.1.1. The hippocampus and mesial temporal lobe epilepsy

The hippocampus is in the medial temporal lobe and is considered a key component of the brain. It is involved in short-time memory, long-time memory and has a crucial role in spatial memory [9]. This structure displays a variety of neuronal cells, that can fire bursts of action potentials, and is considered to be a seizure-prone structure [10].

Mesial temporal lobe epilepsy (MTLE) is one of the most common types of focal epilepsy. It is associated with traumatic brain injury (TBI), head trauma or infection, as some studies have proven these to increase the probability of developing MTLE [11,12]. Most patients diagnosed with MTLE have hippocampal abnormalities, known as hippocampal sclerosis, characterized by extensive gliosis and neuronal loss in the hippocampus, mainly in the cornus ammonis 1 (CA1), dentate hilar region and dentate gyrus (DG) [13,14]. Mossy fiber sprouting is also a common feature of MTLE patients. This consists in an abnormal growth of the axons of the DG granular cells (synaptic reorganization). Mossy fiber sprouting relation to seizure generation has been greatly studied [15]. In MTLE seizures are generally drug-resistant, thus, the only successful treatment to eliminate them is the surgical removal of the mesial temporal structures, as it has been proven successful in up to 80% of the cases [16,17]. Nevertheless, it is still unclear if epilepsy is caused by hippocampal sclerosis (shrunken hippocampus exhibiting neuronal loss) or by spontaneous seizures that lead to neuron damage [12].

1.2. Models of epilepsy

Epileptogenesis is hard to study in humans, due to the multiple and heterogeneous epileptogenic injuries, long latent periods lasting months to decades, and the misleading effects of anticonvulsant treatment

after the first spontaneous seizure. Indeed, clinical trials with humans and human sample studies are still not very effective.

Animal models of epilepsy can mimic several aspects of the disease and were crucial in the identification of AEDs. Studies within these models are the standard procedure in the research regarding epilepsy, and have brought important insides in the molecular, cellular, and electrophysiological processes of epilepsy [18].

For animal models of epilepsy, the most common animal used is the rodent (either mice or rat), in both *in vivo* and *in vitro* experiments. *In vivo* models are divided into categories, according to the type of agent causing epilepsy, namely, chemical (pilocarpine or kainic acid induced models), electrical stimulation (like the kindling model) and genetic (usually mutations associated with ion channels dysfunction) [19,20]. Unlike *in vitro* models, *in vivo* allows the execution of behaviour and motor assessment experiments, but they require more animals, more animal handling expertise and are costly and time-consuming procedures [21]. *In vitro* models allow the study of epilepsy development in simpler systems, like brain slices that contain the cell types present in the brain and maintain the three-dimensional structure of the tissue, allowing the connectivity between cells and the possibility to generate seizures [22]. Brain slices can be acute, meaning that they last some hours in an *ex vivo* environment, and organotypic, which can be maintained in culture for up to 30 days [23]. Moreover, *in vitro* models have the benefit of reducing animal suffering and do not require animal handling.

1.2.1. Models of epilepsy in organotypic slices

Organotypic hippocampal slice cultures (OHSC) are a method of *in vitro* brain tissue culturing that was first introduced by Gähwiler in 1981 [24]. Gähwiler developed the roller tube method, in which slices were embedded in a collagen matrix in glass coverslips under slow rotation. Another technique shortly appeared, as in 1991, when Stoppini and co-workers developed the interface method, where slices were cultured in semiporous membranes [22,24].

OHSC usually contain the hippocampal areas and are prepared using P0 to P7 Sprague-Dawley pups. Early postnatal pups are easier to dissect, the cytoarchitecture of the brain is already established and the cells are more likely to survive explantation [25]. Beside from the hippocampus, organotypic slices can be performed from areas like the cerebellum [26], spinal cord [27] or striatum [28,29], but OHSC are the most used ones. OHSC retains the cellular architecture of the hippocampus, thus preserving the *in vivo* features like neuronal connectivity, synaptic plasticity and chemical signalling. Tissue slicing trauma is reported to cause cell death, however, long term isolation (about 2 weeks in culture), allows the slice to recover, as the tissue debris and dead cells are washed away [24,30].

OHSC share many epileptogenic alterations with human epileptic tissue, and amongst them, neuronal death and seizure generation are the most prevalent ones. Often, deafferentation induced by slicing is associated with neuronal reorganization, as observed in human epileptic patients, where axons form aberrant connections in the sprouting process, leading to hyperexcitability [31–33]. In consequence of these conditions, excitatory activity and localized neuronal hippocampal cell death (mainly in CA1) occur over time in culture [34,35]. OHSC is a multicellular model with features that relate to their *in vivo* counterparts, making it a good model to study physiology, pharmacology and morphology, as well as a method of screening new therapeutic approaches for epilepsy.

However, clinical research and animal models of epilepsy have suggested that the rhinal cortex, composed by perirhinal and entorhinal cortices, plays a role in seizure generation [36]. Thus, a model of epileptogenesis in rhinal cortex-hippocampus organotypic slices was established [37,38]. Under a gradual

and controlled deprivation of serum, rhinal cortex-hippocampus organotypic slices depict evolving epileptic-like events, unlike analogous slices always kept in a serum-containing medium. In this system, epileptic-like activity appears to develop faster than in organotypic hippocampal slices. This might be attributed to the presence of the rhinal cortex, which preserves most of the functional input to the hippocampus. As OHSC, this system represents an easy-to-use screening platform, where pharmacological interventions targeting specific cellular pathways can be implemented and potential therapeutic targets can be tested.

1.3. Neuroinflammation

Inflammation is an immune response to any kind of bodily injury. In the CNS, this response is unique. The CNS has its own immune cells (microglia and astrocytes) which ensure the immune responses, and systemic immune cells like macrophages and neutrophils cannot cross the blood brain barrier (BBB) [39].

Inflammation is usually a beneficial process, with either protective actions against infection or regenerative properties to damaged tissue. While inside the BBB, most lesions are internal and with the skull and BBB intact there are no infections. Hence, in most cases of brain inflammation, recent studies have shown the protective and regenerative actions of inflammation in the CNS, since neurons do not have regenerative abilities on their own [40]. However, when the magnitude or duration of inflammation exceeds the homeostatic threshold, it becomes chronic and it is nowadays considered a trigger for neurological diseases like AD, PD or epilepsy [41].

In the case of epilepsy, recent studies have shown a positive feedback loop between brain inflammation and epileptogenesis caused by inflammation [42]. Chronic inflammation leads to an upregulation of inflammatory cytokines like Interleukin (IL)-1β (IL-1β) and High Mobility Group Box 1 (HMGB1) and activation of Toll-like receptors (TLR), mainly TLR4. This chain of events culminates in the reduction of gamma aminobutyric acid and Ca^{2+} influx, increasing neuronal excitability and decreasing seizure threshold and BBB breakdown [43,44].

1.4. Cytokines

Cytokines are involved in innate and adaptative immune responses and are the main inflammatory regulators of the body. In the innate immune response, pattern recognition receptors (PRR) interact with pathogen associated molecular patterns (PAMPs) identified in pathogens or damage associated molecular patterns (DAMPs) released in tissue damage, where pathogens do not intervene [45]. This recognition initiates a cascade of events that lead to cytokine release. Cytokines then interact with their complementary receptors, inducing a specific response in the target cells. In the CNS, cytokines have a relatively low expression and only become upregulated when inflammatory stimulus is presented [46]. The responses of cytokines to insult, can be either neurodegenerative in case of chronic inflammation, or protective in case of resolution of tissue damage or infection [45]. Some studies have also shown a role of cytokines in synaptic reorganization and plasticity [47].

In epilepsy, cytokine's levels are often higher than normal causing excitotoxicity, neuronal death and synaptic dysfunction, which are common features of the epileptogenesis process and during seizures [48]. Therefore, cytokines facilitate seizure generation, which per se, helps increase cytokine release from cells. They also have a role in various types of programmed cell death in epilepsy, specifically targeted to neurons and in decreasing seizure threshold causing synaptic disfunction. In epilepsy, the main cytokines that intervene in the propagation and onset of the disease are IL-1β, tumour necrosis factor alpha (TNF-α) and IL-6 [49].

1.4.1. IL-1β

IL-1β is the most studied cytokine involved in the inflammatory processes in the CNS. It is the first and main cytokine released under pathological conditions, increases the expression and release of other cytokines and has cell type-specific signalling responses [50]. This cytokine is produced as an inactive precursor, pro-interleukin-1β (pro-IL-1β), that is further cleaved by the proteolytic enzyme Caspase-1 into its active form IL-1β. This process is mediated by the multi protein complex (MPC) inflammasome, which cleaves the enzyme to its proteolytical active state [51].

IL-1β activates its complementary receptor interleukin-1 receptor 1 (IL-1R1) and induces the release of HMGB1 which activates TLR4. These interactions enhance calcium influx by the phosphorylation of *N*-methyl-D-aspartate (NMDA) receptor subunit 2B (NR2B). As IL-1R1 is expressed in glial cells and hippocampal pyramidal neurons, the calcium efflux can lead to neuronal excitability and excitotoxicity [43,50,52]. After the recognition of IL-1β, the signal can trigger several intercellular pathways, like the activation of neuronal factor kB (NF-kB) and mitogen-activated protein kinases (MAPKs), among others [50].

After events of infection or inflammation, the host usually responds with fever. Occasionally, fever causes convulsions (febrile seizures) with the influence of IL-1β, by mechanisms not yet understood. However, it is proven that administration of high doses of IL-1β in the brain of rodents can generate or worsen seizures and the ablation of IL-1R1 gene, gives them resistance to experimental febrile seizures [53].

In physiological conditions various cells in the CNS can release IL-1β, but the main contributor to this supply is microglia. Under pathological conditions, microglia and astrocytes undergo reactive gliosis with exacerbated production and activation of IL-1β [40]. Seizure generation also evoke IL-1β production, and the expression of IL-1R antagonist (IL-1RA) increases to counteract the cytokine's effect. Though, under this pathological situation IL-1RA production is not sufficient and comes with a delay [54,55]. Thus, the brain is not very efficient in evoking a mechanism to cease the neurotoxic effects of IL-1β, because IL-1R1 levels rise significantly in hippocampal neurons after seizures [48].

BBB permeability is also affected by IL-1β. When IL-1β is produced during epileptogenesis it promotes the breakdown of the BBB [48]. This causes the BBB to become permeable to several molecules and cells, like serum albumin and cells of the innate and adaptative peripheral immune system. These cells contribute to perpetuate inflammation and proteins like albumin are responsible for reducing glutamate reuptake by astrocytes leading to chronic neuronal hyperexcitability [43,48].

Collectively, all evidence points to a role of IL-1β as a contributor to the epileptogenic process, decreasing the seizure threshold by an increase in neuronal excitability.

1.5. Inflammasomes

The cytosolic multiprotein complexes known as inflammasomes are usually invested in innate immune responses. They were first discovered by Martinon and colleagues in 2002 [51] and are responsible for the activation of pro-inflammatory caspases. The term inflammasome is only considered when the oligomer is connected to a Caspase-1 activating complex [51]. These types of multiprotein complexes have proven to be a crucial component to innate immunity and for host protection [56].

As mentioned before, the inflammasomes trigger the activation of Caspase-1 that subsequentially trigger pro-inflammatory cytokine cleavage and release, leading to and inflammatory response. The cell pathways, that lead to such response, promote neuronal death by pyroptosis, a pro-inflammatory process

mediated by gasdermin D (GSDMD) (see section 1.6.1) [57]. Therefore, inflammasome can drive the inflammatory response, either to the repair of damaged tissue or promotion of pathological conditions like AD, traumatic brain injury, multiple sclerosis (MS) and epilepsy [58–60].

Inflammasomes are divided in 3 main components, a PRR that acts like the sensor molecule, the adaptor apoptosis-related speck-like containing a caspase recruitment domain protein (ASC) and the effector pro-caspase-1 [61]. ASC contains a pyrin domain (PYD) and a caspase activation and recruitment domain (CARD), acting as an adaptor between the PYD of the sensor protein and the CARD of pro-caspase-1. Nonetheless, there are minor disparities in the structure between different types of inflammasomes [62].

PRR are expressed in various types of cells in the CNS (microglia, astrocytes, oligodendrocytes, amongst others) [63] and are subdivided into two major classes: transmembrane and intracellular proteins [64]. TLR and C-type lectin receptors (CTL) are transmembrane proteins that detect alterations in the extracellular environment. In the subsequent class, RIG-I-like proteins (RLR), AIM2-like-receptor (ALR) and the nucleotide binding domain and leucine rich repeat containing (NLR) proteins [65] scan the intercellular milieu and are engaged in inflammasome formation, further explain ahead [66].

The NLR family is subdivided in 4 sub-families, according to the N-terminal domain they contain. NLRA for the acidic domain, NLRB for the baculoviral inhibitory repeat (BIR) domain, NLRC for the CARD domain and NLRP for the PYD [65]. These types of PRR also contain a C-terminal leucine-rich domain (LRR) and a central nucleotide-binding and oligomerization domain (NATCH). The N-terminal domain mediates downstream signalling transduction while the central NATCH domain has ATPase activity and is vital in the formation of oligomeric structures. Lastly, the LRR functions as an autoregulatory component serving as a ligand interactor [62].

Every NLR reacts and elicits a response, depending on the type of PRR they possess. The stimuli received are either PAMPs or DAMPs released from damaged cells. Most of the NLR react to at least one of them. NLRP1 is activated by *Bacillus anthracis* lethal toxin (LeTx) and bacterial muramyl dipeptide (MDP), whereas NLRC4 responds to cytosolic flagellin from Gram-negative bacteria. AIM2 responds to dsDNA, either viral, bacterial, or self-DNA and finally, NLRP3 senses several PAMP's and DAMP's, further specified ahead [56,62,67].

1.6. The NLRP3 inflammasome

Within the NLRs, the NLRP subfamily is the biggest one, comprising 14 members [68]. Within the NLRPs, the NLRP3 inflammasome is the best described one. It is encoded by the nlrp3 gene and is often referred to as NATCH, LRR and PYD domains-containing protein 3, cryopyrin, NALP3 or nucleotide-binding oligomerization domain. It is composed by a sensor NLRP3, an adaptor (ASC) and an effector (Caspase-1). The sensor domain is composed of 3 subdomains: (1) an C-terminal LRR with autoinhibitory function; (2) a central NATCH with ATPase activity, vital to inflammasome assembly; (3) a N-terminal PYD responsible for ASC connection in NLRP3 assembly [69].

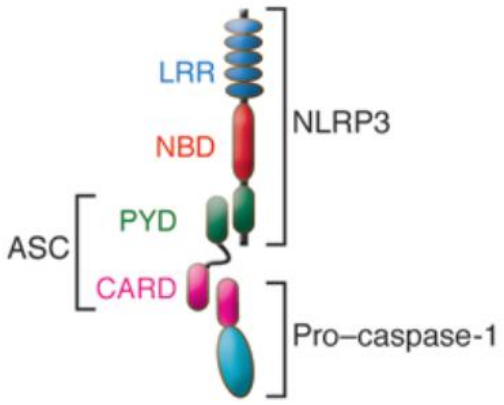

Figure 2.1: NLRP3 inflammasome structure representation. Adapted from Stutz, et al. 2009.

Mutations in the sensor domain are responsible for the inherited cryopyrin-associated periodic syndromes (CAPS). Familial cold autoinflammatory syndrome (FCAS), Muckle-Wells syndrome (MWS) and neonatal-onset multisystem inflammatory disease are some diseases included in CAPS [70]. Nevertheless, alterations in the normal activation of NLRP3 can lead to other diseases, including gout, AD, MS, TBI and type 2 diabetes [70,71].

Which brain cells express NLRP3 is still a debated subject. Even though there are numerous articles concerning the NLRP3 inflammasome, few discuss its location. Still, it is important to distinguish location of inflammasome components and sites where it is activated. It is accepted that NLRP3 components exist in microglia and can be assembled into active NLRP3 under pathological conditions [60,72,73]. However, there is also evidence of NLRP3 expression in oligodendrocytes [74], spinal cord astrocytes [75], and neurons [76,77]. ASC and Caspase-1 are poorly expressed in primary cortical neurons [73] and ASC expression is also described in disease models [76]. Altogether, the evidence suggests the presence of all NLRP3 components in neurons, suggesting that inflammasome activation may occur in these cells. Nevertheless, further studies are required to clarify and eventually discover new sites of inflammasome activation.

1.6.1. Inflammasome assembly and activation

NLRP3 inflammasome can recognize several stimuli, that initiate the first step (priming) of the most consensual mechanism of NLRP3 activation (canonical pathway), like lipopolysaccharide (LPS), MDP and bacterial or viral RNA [67,70]. The priming step upregulates the transcription of NLRP3 domain and pro-IL-1β, which basal expression is very low, through activation of NF-kB [78]. TLR4 and its modulator Myd88 also intervene in the post-translational modifications that prime NLRP3, namely its de-ubiquitination by BRCC3 (JAMM domain containing Zn2+ metalloprotease) [70,79].

The second step begins once the inflammasome is primed, being provided by adenosine triphosphate (ATP), uric acid crystals, bacterial pore-forming toxins, fungal or protozoan pathogens, amongst other [78]. The molecular and cellular events that lead to the inflammasome activation are still debated. The numerous NLRP3 inflammasome-activating stimuli are highly different at the chemical and structural level, so it is unlikely that they physically interact with NLRP3 [76]. The occurrence of a common signal generated by NLRP3 activators was thus proposed, such as K^+ efflux, Ca^{2+} signalling disturbance, toxin-mediated membrane disruption, reactive oxygen species (ROS) production, mitochondrial dysfunction and lysosomal rupture [69,79]. Between these, K^+ efflux is the most well-known activator of the inflammasome. Extracellular ATP has been proposed to activate P2X purinergic receptor 7 (P2X7) which, per se, controls NLRP3 activation through the upregulation of Ca^{2+} and Na^{2+} influx, directing the K^+ channel two-pore domain weak inwardly rectifying K^+ channel 2 (TWIK2), to mediate K^+ efflux [80]. Moreover, low intracellular concentrations of K^+ are enough to cause spontaneous NLRP3 inflammasome activation [81,82]. In recent studies, a new protein that regulates NLRP3 activation downstream of K^+ efflux has emerged, Nek7, a serine/threonine protein kinase related to mitosis progression, binds to the LRR of NLRP3 and is necessary to ASC oligomerization and Caspase-1 activation [83,84].

Following ASC recruitment, NLRP3 forms ASC filaments that meld into a macromolecule known as ASC speck. When this structure binds to sensor proteins, it can recruit pro-caspase-1 through CARD-CARD interactions and facilitates Caspase-1 self-cleavage and activation [85]. When Caspase-1 is active, it mediates the cleavage of pro-IL-1β and pro-IL-18 into active inflammatory cytokines and can also release the N-terminal domain of GSDMD leading to the inflammatory cell death, pyroptosis (see section 1.7.1).

Shortly, the alternative inflammasome activation pathway (non-canonical pathway) acts through a Caspase-11-mediated NLRP3 activation, leading to the release of IL-1β and IL-18 and to a NLRP3-independent pyroptosis via GSDMD N-terminal domain [79,86]. While it is known that most Gram-negative bacteria activate Caspase-11, the mechanisms upstream its activation continue to be debated. As Gram-positive bacteria cannot activate this pathway, LPS was suggested by some studies to intervene in this inflammasome activation mechanism. As Kayagaki and Hagar have shown, LPS binds to the CARD domain of Caspase-11 and activates it, independently of TRL4, where, in the canonical pathway, LPS usually binds [87,88].

1.7. Cell death

Cell death is the final solution for a cell when numerous stresses are accumulated up to a level beyond the cell's recovery capacity. In the CNS, neuronal death is a natural occurrence, mainly during development, but neurons die at a much higher rate in brain diseases, like AD and epilepsy [89,90]. In epilepsy, neuronal death is directly associated with seizure generation and seizure-induced neuronal death in epileptogenesis is a highly controversial area and heavily studied by neuroscientists [91]. Indeed, in animal models, induced *status epilepticus* (SE) was proven to incite neuronal death and lead to chronic epilepsy. Consequently, neuronal death is a direct effect of epileptogenesis in SE models [90].

Neuronal damage is usually associated with excitotoxicity, which is caused by an increase in glutamate release or decrease in its reuptake by astrocytes, that subsequently binds to glutamate receptors in excitatory synapses [92]. Excitotoxicity often leads to various types of cellular death, namely, apoptosis, necrosis, or pyroptosis, occurring in several types of cells in the CNS [91,93]. Apoptosis is a programmed type of cell death initiated by stress signals, that results in Caspase-3 activation and mitochondrial release of cytochrome c. The cell collapses into several membrane enclosed vesicles, known as apoptotic bodies, that contain the spread of inflammation [94]. In contrast, necrosis is caspase independent. This type of cell death is an accidental unprogrammed process caused by factors external to the cell or tissue, such as infection or trauma, and ends in cell lysis and release of cell contents, damaging the surrounding cells [95].

1.7.1. Pyroptosis

A pro-inflammatory type of cell death, caused by Salmonella and Shigella species and dependent on Caspase-1 was identified by several investigators [96,97]. Recent studies show that this process is associated with a variety of diseases, including CNS diseases [98]. Caspase-1 is not involved in apoptosis [99], however, its activation in macrophages lead to IL-1β and 1L-18 activation and host cell death [100]. This evidence implied that there was another kind of regulated cell death distinct from apoptosis. Fink and colleagues in 2005, proposed the term pyroptosis to describe this new type of cell death [101]. This is an inflammatory type of cell death characterized by nucleus pycnosis, DNA fragmentation, cell swelling, membrane rupture and release of cytosolic content [57].

Pyroptosis was long regarded as a Caspase-1-mediated cell death but was redefined as a GSDMD-mediated programmed cell death [102]. Recent observations confirmed that the pyroptosis executioner, GSDMD, is also a substrate of inflammatory Caspases-11 (in murine) and Caspases-4/5 (in human). The involvement of inflammatory caspases is the main mechanism that distinguishes pyroptosis from other kinds of cell death. GSDMD belongs to a family of pore-forming proteins and mediates pyroptosis after undergoing cleavage by inflammatory caspases, producing an N-terminal fragment that can form pores in the plasma membrane and a C-terminal with autoinhibitory characteristics [103,104]. The creation of membrane pores leads to blebbing, producing protrusions called pyroptotic bodies, that later burst and release their content. Here, pyroptosis distinguishes itself from necrosis, where the membrane

immediately bursts, and from apoptosis where the apoptotic bodies formed are safely digested by macrophages or microglia [91]. Although GSDMD is constitutively expressed, its upregulation can be triggered by exposure to inflammatory cytokines to enable pyroptosis [105]. In the CNS, numerous cells can undergo pyroptosis, as neurons, microglia, astrocytes, amongst others, with the difference being the pathway that triggers the process, either the inflammatory caspase that can directly cleave GSDMD, as for example Caspase-1/Caspase-11 that are present in the canonical/non-canonical pathway of NLRP3 activation, or the inflammasome involved, as different inflammasomes assemble in different cell types [60,106,107].

Pyroptosis can intervene in several pathologies of the CNS, including AD [106,] brain and microbial infections like sepsis-associated encephalopathy (SAE) [108], MS and PD [109]. However, evidence is arising that inhibition of Caspase-1-activating inflammasomes, as NLRP3, can have benefits in the impairment of several diseases [110,111]. In epilepsy, pyroptosis involvement is still under debate with studies showing a connection between this disease and inflammasome-induced cell death. More specifically, evidence shows that NLRP3 or Caspase-1 silencing in kindling-induced rat model or pharmacological inhibition of NLRP1 in intrahippocampal kainite-induced rat model of MTLE, were effective potential therapies upstream of pyroptosis [112,113].

1.8. MCC950 as a selective NLRP3 inflammasome inhibitor

NLRP3 inflammasome is, by far, the best studied and most characterized inflammasome. Aberrant activation of this complex and IL-1β/IL-18 secretion has been implicated in various diseases [71], including inflammatory diseases, diabetes, atherosclerosis, and neurodegenerative diseases, evoking a substantial clinical interest in exploring the effectiveness of its inhibitors.

In 2001, several IL-1 post-translational processing inhibitors, also called cytokine release inhibitory drugs (CRID) were identified [114]. Indeed, the inhibition of inflammasome end products has proven to be successful in several inflammatory disease treatment [115]: Canakinumab, a humanized antibody against IL-1β and rilonacept, a soluble decoy IL-1 receptor, were developed to treat CAPS; or anakinra, an recombinant IL-1RA, helpful when dealing with rheumatoid arthritis (RA) [70]. In epilepsy refractory patients, there are reports of controlled seizures following anakinra administration [116,117]. Also, there are reports that the carotenoid astaxanthin (AST) had strong anti-inflammatory effects and downregulated P2X7 receptor in microglia [118]. Interfering with IL-1β production was proven to tangle with seizures. In animal models, intrahippocampal administration of IL-1RA effectively reduced seizure incidence [119]. In 2014, Meng and colleagues proved that infusion of non-viral small interfering RNA, to knock down NLRP3 and Caspase-1 in the brain of SE rats, led to a substantial reduction in seizure generation and severity, decrease in IL-1β levels and strong reduction of hippocampal neuronal loss [120].

Several other NLRP3 inhibitors have been reported, either targeting NLRP3 directly or indirectly inhibiting its activation. For example, glyburide and FC11A-2 indirectly inhibit inflammasome activation by inhibiting ASC aggregation and interfering with pro-Caspase-1 autocleavage, respectively [121]. MCC950, a diarysulfonylurea-containing compound, was described by Coll and colleagues in 2015 as a selective inhibitor of NLRP3. It inhibits both canonical and non-canonical pathways through the blockage of NLRP3-induced ASC oligomerization. It interacts with NLRP3 near the Walker B motif, which intervenes in ATP hydrolysis, blocking this function [122]. MCC950 also counteracts the structural rearrangements that NLRP3 undergoes in its activation by driving NLRP3 to an inactive form [123]. This small molecule is capable of inhibiting NLPR3, at micromolecular concentrations, but not other inflammasomes as NLRC4, AIM2 or NLRP1. Thus, it still allows inflammatory responses and IL-1β production by other inflammasomes, reducing the immunosuppressive effect that other drugs have [110].

The pharmacokinetic profile of MCC950 has already been determined. It is a stable compound, with a half-life of 3.27 h and bioavailability of 68%. More than 70% of the compound remains in liver microsomes after 60 min and the drug-drug interaction potential was tested with 5 major cytochrome P450 enzymes with its inhibition being less than 15% [110].

Promising results suggest that MCC950 is effective in inhibiting NLRP3 in a mouse model of Muckle-Wells syndrome and greatly ameliorates the severity of experimental autoimmune encephalomyelitis (EAE) in a model of human MS [110]. MCC950 also helps prevent the progression of several diseases, including autoimmune diseases. Altogether, evidence suggests that this compound has a potential clinical use, although further studies are necessary to clarify its inhibitory and prospective use in humans [124].

2. Aims

In epilepsy, neuronal death is directly associated with seizure generation and the role of seizure-induced neuronal death in epileptogenesis is a highly controversial topic [91]. In addition, the involvement of NLRP3 inflammasome mediated cell death (pyroptosis) in epilepsy is still under debate.

Epileptic-like rhinal cortex-hippocampus organotypic slices at 14 DIV show increased cell death when compared with slices that do not depict epileptiform activity [37]. In this work we further explored this system trying to disclosure the relationship between NLRP3 inflammasome signalling and pyroptosis to the progression of the epileptic-like events.

Therefore, this study aimed to 1) characterize the development of epileptiform activity, 2) address the occurrence of NLRP3-mediated neuronal death by pyroptosis and 3) assess the impact of an inflammasome inhibitor, MCC950, in epileptiform activity. To achieve such goals, techniques as electrophysiological recordings and molecular-based assays were applied in epileptic-like rhinal cortex-hippocampus organotypic slices (from now on named EL slices for simplification) to evaluate several topics throughout time in culture:

- Spontaneous epileptiform activity
- Cell death
- ROS production
- Co-localization of NLRP3 components in neurons
- IL-1β release

3. Materials and Methods

3.1. Animals

Six to seven-days old Sprague-Dawley pups were used to prepare rhinal cortex-hippocampus organotypic slice cultures. Pregnant rats were obtained from Charles River Laboratories (Barcelona, Spain). All procedures were performed according to the current Portuguese Law and European Union guidelines (2010/63/EU) regarding the protection of animals used for scientific purposes. Experimental approval was granted by the iMM's Institutional Animal Welfare Body (ORBEA-iMM) and the National competent authority (DGAV – Direção Geral de Alimentação e Veterinária). All experiments were performed using the minimum number of animals possible to reduce animal suffering.

3.2. Rhinal cortex-hippocampus organotypic slice cultures

Rhinal cortex-hippocampus slices were prepared from 6-7-days old Sprague-Dawley pups. Rats were euthanized by decapitation and the brain removed to a 60 mm plate with ice cold Gey's balanced salt solution (GBSS) (Biological Industries, Israel) supplemented with 25mM D-glucose (Sigma-Aldrich, USA). Under sterile conditions, forceps was inserted between the eye sockets to hold the head and, using thin scissors, the skin was cut along the midline, from the vertebral foramen towards the frontal lobes. Next, the skull was cut in the same way and along the cerebral transverse fissure, using curved forceps to expose the brain. The olfactory bulbs were discarded with the help of a spatula and the brain was transferred to a new dish with ice-cold GBSS. Under the dissection microscope, both hemispheres were separated along the midline and excess tissue was removed to expose the hippocampus. Hemispheres were placed, with hippocampus parallel to each other and facing up, in a filter paper. Tissue was cut perpendicular to the blade into 350 µm thick slices in a McIlwain tissue chopper. Sliced tissue was placed in another culture dish with cold GBSS and slices were carefully separated using round-tip glass electrodes to prevent damaging the slices. Only the slices that displayed a structurally intact hippocampus and perfectly defined DG and CA areas were collected. Generally, 6 to 10 slices per hemisphere were structurally intact and undamaged to be collected and placed in a porous (0,4 µm) insert membrane (EDM Millipore, USA), in six-well culture trays (Corning, USA). Each well contained 1.1 mL of culture medium composed of 50% Opti-MEM, 25% Hanks' balanced salt solution (HBSS), 25% heat-inactivated horse serum (HS), gentamycin 30µg/mL (all from Invitrogen, UK), and 25 mM D-glucose. Slices were maintained at 37ºC with 5% CO_2 and 95% atmospheric air for the following 3 weeks. From 3 days in vitro (DIV) on, slices were changed to supplemented Neurobasal A medium (NBA: 2% B-27, 1mM L-glutamine and gentamycin 30µg/mL, all from Invitrogen, UK) and subjected to decreasing HS concentrations (15%, 10% and 5%) until a serum free medium was reached at 9 DIV [37].

Culture maintenance was performed every 2-3 days and at every change, the medium was collected in cryogenic vials (Corning, USA) for ELISA. At 7, 14 and 21 DIV slices were fixed and kept at 4ºC for immunohistochemistry assays or hippocampal tissue was collected in cryogenic vials and stored at -80ºC until further processing. Electrophysiological recordings were performed at 6-8, 13-15 and 20-22 DIV.

3.3. Cell death assessment by propidium iodide uptake

Cell death was assessed by the cellular uptake of a red fluorescence dye, propidium iodide (PI, 3,8-diamino-5-(3-(diethylmethylamino) propyl)-6-phenyl phenanthridinium diiodide, Sigma-Aldrich, USA). PI is a polar compound that interacts with DNA emitting red fluorescence (630 nm; absorbance 493 nm). It is only permeable to compromised cell membranes, thus only cells with damaged membranes can be identified with PI. PI is not toxic to live cells, therefore, it was used to identify cell death in organotypic slices.

From PI stock solution (1.5mM), a 1:10 dilution was made and 13µL of diluted PI were added to the medium of each insert, to a final concentration of 2µM. After a 2 h incubation period (37ºC, 5% CO_2 and 95% atmospheric air) images were acquired under a wide field fluorescence microscope (Axiovert 200, Zeiss, Germany) with a 5x magnification. PI uptake assay was performed in slices at 3, 7, 14 and 21 DIV and the fluorescence intensity was quantified using ImageJ Software (National Institutes Health, USA), individualizing each area of interest (DG, CA3 and CA1). The intensity value of each analysed region was obtained by correction with a fluorescence background image. PI uptake by each

hippocampal region was expressed in arbitrary units of fluorescence intensity. After image acquisition, slices were fixed for immunohistochemistry (explained in section 3.5).

3.4. Reactive oxygen species quantification

DCFDA (2,7-dichlorofluorescin diacetate) is a fluorescent dye that measures ROS in the cell. Once in the cell, it gets deacetylated into a non-fluorescent compound that is oxidized posteriorly, by ROS, into the fluorescent DCF (2,7-dichlorofluorescein; 495 nm, absorbance 529 nm). As a result, fluorescence intensity is proportional to the amount of ROS present in the samples.

A 2mM solution of DCFCA was prepared in the buffer provided by the manufacturer (ab113851, Abcam, UK). At 3, 7, 14 and 21 DIV, 5µL of DCFDA solution was added into the medium of each insert, to a final concentration of 10µM. After 30 min of incubation (37ºC, 5% CO_2 and 95% atmospheric air), the medium was removed, and three washes with phosphate buffered saline (PBS) were performed. Images were acquired under a wide fluorescence microscope (Axiovert 200, Zeiss, Germany) with a 5x magnification. Fluorescence intensity was quantified using ImageJ Software (National Institutes Health, USA) individualizing the areas of interest (DG, CA3, CA1). The intensity value of each analysed region was obtained by correction with a fluorescence background image. DCF fluorescence of each hippocampal region was expressed as percentage of 3 DIV.

3.5. Immunohistochemistry

Slices were fixed at 7, 14 and 21 DIV in 4% paraformaldehyde (PFA, Sigma-Aldrich, UK) diluted in PBS for 1 h at room temperature (RT) followed by two PBS washes. Slices were maintained in PBS at 4ºC until further use. PFA and PBS (1 mL) were added above and beneath the inserts.

Slice were individualized from the insert, with a sharp scalpel, and transferred to slides. Each slice was surrounded with a hydrophobic pen (Dako, Denmark) to reduce solution volume to a minimum and to protect the slices from drying.

Following PBS washes, permeabilization / blocking solution composed of 10% bovine albumin serum (BSA), 10% HS and 1% triton X-100 in PBS, was added to each slice. After a 3 h incubation period at RT and three PBS washes, the slices were incubated with the primary antibodies, diluted in 5% BSA in PBS, overnight at 4ºC. Slices were then washed with PBS with 0.1% Tween-20 (PBST) and the fluorophore-coupled secondary antibodies, diluted in PBS, were added for a 4 h period at RT. Cell nuclei were stained with HOECHST 33342 (20 µg/mL, Invitrogen, UK) for 20 min and slices were mounted with mowiol and sealed with nail polish. After at least 24 h, images were obtained on an inverted confocal laser scanning microscope (Zeiss LSM 710, Zeiss, Germany) under a 20x magnification objective (with 0.6 times digital zoom out, equivalent to 12x magnification) and 40x digital zoom.

The primary antibodies used were mouse anti-NeuN (1:500, MAB377, Millipore SAS), rabbit anti-NeuN (1:500, 16712943S, Cell Signalling, USA), rabbit anti-NLRP3 (1:500, ab214185, Abcam. UK), rabbit anti-ASC (1:750, AG-25B-0006, Adipogen) and rabbit anti-GSDMD (1:200, ab209845, Abcam, UK). The secondary antibodies used were donkey anti-mouse and donkey anti-rabbit coupled to Alexa Fluor 488 and donkey anti-mouse and donkey anti-rabbit coupled to Alexa Fluor 568 (1:500, Invitrogen, UK).

3.6. Enzyme-linked immunosorbent assay (ELISA)

Medium was collected from slices at 3, 6, 7, 8, 10, 13, 14, 15, 17, 20 and 21 DIV to quantify the IL-1β released. The experiment was performed following the manufacturer's protocol kit (DY008, R&D Systems, UK) using a selective antibody that recognizes both pro-IL-1β and IL-1β.

96-well plates were coated with Capture Antibody (CA) (working concentration of 0.8 µg/mL of goat anti-rat IL-1β in PBS) and incubated overnight at RT. During this period, the antibody will bind to the polystyrene wells. On the following day, CA was discarded, the wells were washed three times with wash buffer and blocking solution (RD) was added for 2 h at RT. After three more washes, two series of IL-1β were prepared: 1) diluted in Opti-MEM medium (ranging from 1-250 pg/mL), for quantification of 3 DIV samples; and 2) diluted in NBA medium (ranging from 1-1000 pg/mL), for evaluation of all the remaining timepoints. Also, 3 DIV samples were diluted in Opti-MEM, while the remaining samples were diluted in NBA medium. Samples and standards were added to the wells for 2 h. Following the previous incubation period, a Horseradish Peroxidase (HRP)-labelled antibody (detection antibody, working concentration of 0.1 µg/mL) was added for 2 h at RT. This antibody will attach to the IL-1β captured by CA. Three more washes later, streptavidin solution was added for 20 min followed by tetramethylbenzidine (substrate solution) addition, turning the samples colour to blue according to the amount of IL-1β present. The reaction was stopped with 2N of sulfuric acid, which turned the samples colour to yellow. Absorbance was read at 450 nm with a 540 nm reference in the Microplate Reader TECAN Infinite M200 (TECAN Trading AG, Switzerland).

With the data obtained from the IL-1β standards, a calibration curve was created (concentration vs absorbance). Concentration of the samples was calculated using the four-parameter logistic regression (4PL), with GraphPad Prism 8.0.1, derived from the calibration curve of known concentrations of IL-1β.

3.7. Protein extraction and quantification

Within the slices, hippocampal tissue was individualized and mixed with 120µL of lysis buffer (50mM Tris pH 8.0, 5mM EDTA, 150mM NaCl, 1% NP-40, 5% glycerol), supplemented with protease inhibitors (complete Mini-EDTA-free, Roche, Germany) and 1 mM phenylmethylsulfonyl (PMSF, Sigma-Aldrich, UK) to avert protein degradation. Tissue was dissociated by sonication (Sonics & Material Inc) and incubated at 4ºC with slow agitation for 15 min. After a 10 min centrifugation period, at 13000 g and 4°C, supernatants were collected and stored at -20ºC until further use.

Total protein quantification was performed using the Bio-Rad DC Protein Assay Kit (Bio-Rad, USA), which is a colorimetric assay for protein concentration following detergent solubilization. Shortly, in a 96-well flat bottom plate, 10µL of diluted samples (1:10) and serial dilutions of BSA (10 dilutions ranging from 0-1µg/mL, used as a protein standard) were distributed through the wells. All dilutions were made in Milli-Q water. On top of samples or standards, 25µL of reagent A' (prepared from reagent A and S together according to the manufacturer´s suggestions) were added, followed by 200µL of reagent B, turning the liquid into a blue tone, proportional to the protein quantity. After 15 min in slow agitation and removal of all air bubbles with a clean needle, absorbances were read at 750nm in the Microplate Reader TECAN Infinite M200.

3.8. Western blot

Samples were mixed with sample buffer (60mM Tris 0.5M pH 6.8, 47% glycerol, 12% sodium dodecyl sulphate (SDS), 600mM dithiothreitol and 0.06% Bromophenol blue) and denatured for 10 min at 95ºC.

Subsequently, samples with 40µg of total protein and molecular weight marker (MWM, NZYColour Protein Marker II, NZYtech, Portugal) were electrophoresed in a 12%, 1.5mm SDS-PAGE gel at 80 volts until the marker starts to separate, and posteriorly at 120 volts for 1h 30 min. Separated proteins were then electrotransferred to polyvinylidene fluoride (PVDF) membranes at a current of 350 milliamperes for 100 min. Membranes were blocked in 3% BSA in Tris Buffer Saline with Tween -20 (TBS-T, 200mM Tris/HCL pH 7.6, 1.5M NaCl and 0.1% Tween-20) for 1h with small agitation. BSA proteins cover the membrane preventing non-specific antibody binding. Soon after, the membranes were incubated overnight at 4ºC with primary antibodies, diluted in 3% BSA in TBS-T, on a rotating shaker. Anti-mouse or anti-rabbit HRP-conjugated antibodies, diluted in blocking solution, were added to the membranes for 1 h at RT with small agitation. Between all steps, membranes were washed for 10 min under small agitation with enough TBS-T to cover them. Immunoreactions were visualized using the ECL Western Blotting Detection System. Chemiluminescence was detected in Image Lab software 5.2.1 associated to Chemidoc MP Imaging System (Bio-Rad, USA). After each detection, membranes were incubated with stripping solution (200mM glycine, 0.1% SDS, 1% Tween-20, 50% acetic acid, pH 2.2) for 30 min under small agitation to remove the previous antibodies from the membranes, allowing re-incubations. After this period, membranes were blocked and re-incubated with antibodies against other antigens.

The integrated intensity of each band was calculated using computer-assisted densitometry analysis with ImageJ software. The image chosen for quantification was the one just before signal saturation. Glyceraldehyde 3-phosphate dehydrogenase (GAPDH) was used to normalise band intensities, correcting possible loading errors. The representative image of each protein evaluated was prepared in Image Lab by merging the chemiluminescence image with the colorimetric image of the MWM.

The primary antibodies used were rabbit anti-NLRP3 (1:500, ab214185, Abcam, UK), rabbit anti-ASC (1:1000, AG-25B-0006, Adipogen), rabbit anti- GSDMD (1:500, ab209845, Abcam, UK), mouse anti-Caspase-1 (1:500, sc-56036, Santa Cruz Biotechnology, USA) and mouse anti-GAPDH (1:5000, AM4300, Ambion).

3.9. Electrophysiology in organotypic slices – Extracellular field potentials

Electrophysiological recordings were obtained in slices with 6-8 DIV, 13-15 DIV and 20-21 DIV. Slices were removed from the incubator and placed on a petri dish with heated NBA medium. A single slice was individualized from the insert, with a sharp blade, and placed in an interface recording chamber with a humidified 95% O_2/5% CO_2 atmosphere at 37ºC. In the interface chamber the medium only passes under the slice, mimicking the conditions of the incubator. The medium was superfused and recirculated at a constant rate of 2 mL/min, allowing the slice to constantly be in contact with fresh medium.

Ictal discharges (bursts), originated in the entorhinal cortex, propagate through DG, CA3 and CA1, while interictal discharges, originated in the CA3 travel, to the CA1, subiculum, entorhinal cortex and re-enter the hippocampus through the DG. Taking into consideration both origin and travel patterns of ictal and interictal discharges, CA3 pyramidal cell layer was the area chosen to monitor the electrical activity of neurons, as it is considered to be the area with the most recurring epileptiform discharges [125,126].

Recordings were performed, for 30 min, using a glass micropipette electrode (2-4MΩ) filled with artificial cerebrospinal fluid (aCSF; 124mM NaCl, 3mM KCl, 1.2mM NaH_2PO_4, 25mM $NaHCO_3$, 10mM glucose, 2mM $CaCl_2$ and 1mM $MgSO_4$; pH 7.4) and were obtained with an Axoclamp 2B amplifier (Axon Instruments, USA), digitized with the WinLTP software (WinLTP Ltd., UK) [127]. Data analysis was performed using the pCLAMP Software version 10.7 (Molecular Devices Corporation,

USA). All results were band-pass filtered (eight-pole Bessel filter at 60 Hz and Gaussian filter at 600 Hz.)

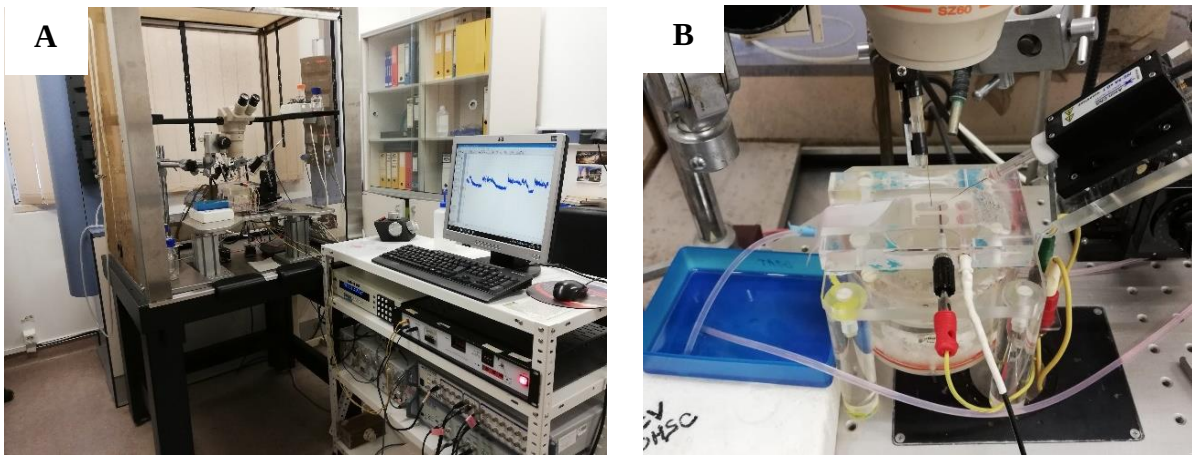

Figure 3.1: Electrophysiology setup. (A) Interface recording chamber and micromanipulators on the left and computer, amplifiers and temperature controller on the right. **(B)** Magnification of the interface recording chamber.

3.10. Characterization of epileptiform activity

In this study, interictal and ictal activity were clearly defined, despite ictal activity being the main focus. Interictal discharges were defined as paroxysmal discharges that were clearly distinguished from background activity, with an abrupt change in polarity occurring within several milliseconds [128]. Ictal-like epileptiform activity was defined as continuous discharges (bursts) lasting more than 10s. Bursts were distinguished when the inter-spike interval was longer than 2s. Continuous activity that did not fit within this parameters was not considered burst activity [38].

Several parameters were assessed to characterize the epileptiform activity of the slices. Number and duration of bursts, frequency of events within a single burst and positive peak positive amplitude (starting from the baseline) were detected by the pCLAMP Software. The number of bursts per slice was detected manually, according to the parameters mentioned above. The baseline was also defined manually to reject any noise oscillations.

3.11. Impact of NLRP3 inflammasome inhibition by MCC950

The impact of the selective NLRP3 inflammasome inhibitor MCC950 [110] (Cayman Chemical Company, USA) was evaluated in 13-15 DIV slices. Recording was performed for 30 min. If the slice did not depict epileptiform activity in this time interval, it was discarded. After 30 min with ictal-like activity, the superfused medium was changed to NBA with freshly added MCC950 (1µM and 5µM), prepared from a 10mM stock solution diluted in dimethyl sulfoxide (DMSO), and the recording proceeded for 1 h more. The impact of MCC950 was evaluated in the number and duration of bursts, frequency of events within a single burst, and positive peak amplitude.

3.12. Statistical analysis

All statistical analysis was performed with GraphPad Prism 8.0.1. Statistical analysis was performed either with unpaired T-test or one-way Analysis of Variance (ANOVA) followed by Tukey's multiple comparison test in N independent cultures or slices. Data were presented as mean ± standard error of the mean (SEM) with statistical significance considered when $p<0.05$.

4. Results

4.1. Characterization of spontaneous epileptiform activity

To evaluate the development of epileptiform activity in slices throughout time in culture, extracellular recordings were performed for 30 min, as explained in section 3.9. Slices at 6-8 DIV (**Fig. 4.1A**) depicted mixed interictal and ictal activity. From 13-15 DIV (**Fig. 4.1B**), epileptiform activity is mainly characterized by ictal discharges, that last more than 1 min at 20-22 DIV (**Fig. 4.1C**). Taking into consideration the parameters chosen to evaluate the epileptiform activity (see section 3.10), 13-15 DIV slices tend to have higher values than 6-8 and 20-22 DIV, except in the average positive peak amplitude of events (**Fig. 4.2C**). The number of bursts per slice was statistically higher than 6-8 DIV (6-8 DIV: 4.88 ± 0.88 vs 13-15 DIV: 13.8 ± 1.39, $p<0.001$) (**Fig. 4.2A**) and the frequency of events per burst (**Fig. 4.2D**) also was statistically higher at 13-15 DIV (13-15 DIV: 9.702 ± 0.822 vs 6-8 DIV: 5.96 ± 0.92, $p<0.05$). Average positive peak amplitude of events does not show differences between the days in culture evaluated. Overall, slices already show signs of spontaneous activity at 6-8 DIV, reaching the peak of activity at 13-15 DIV.

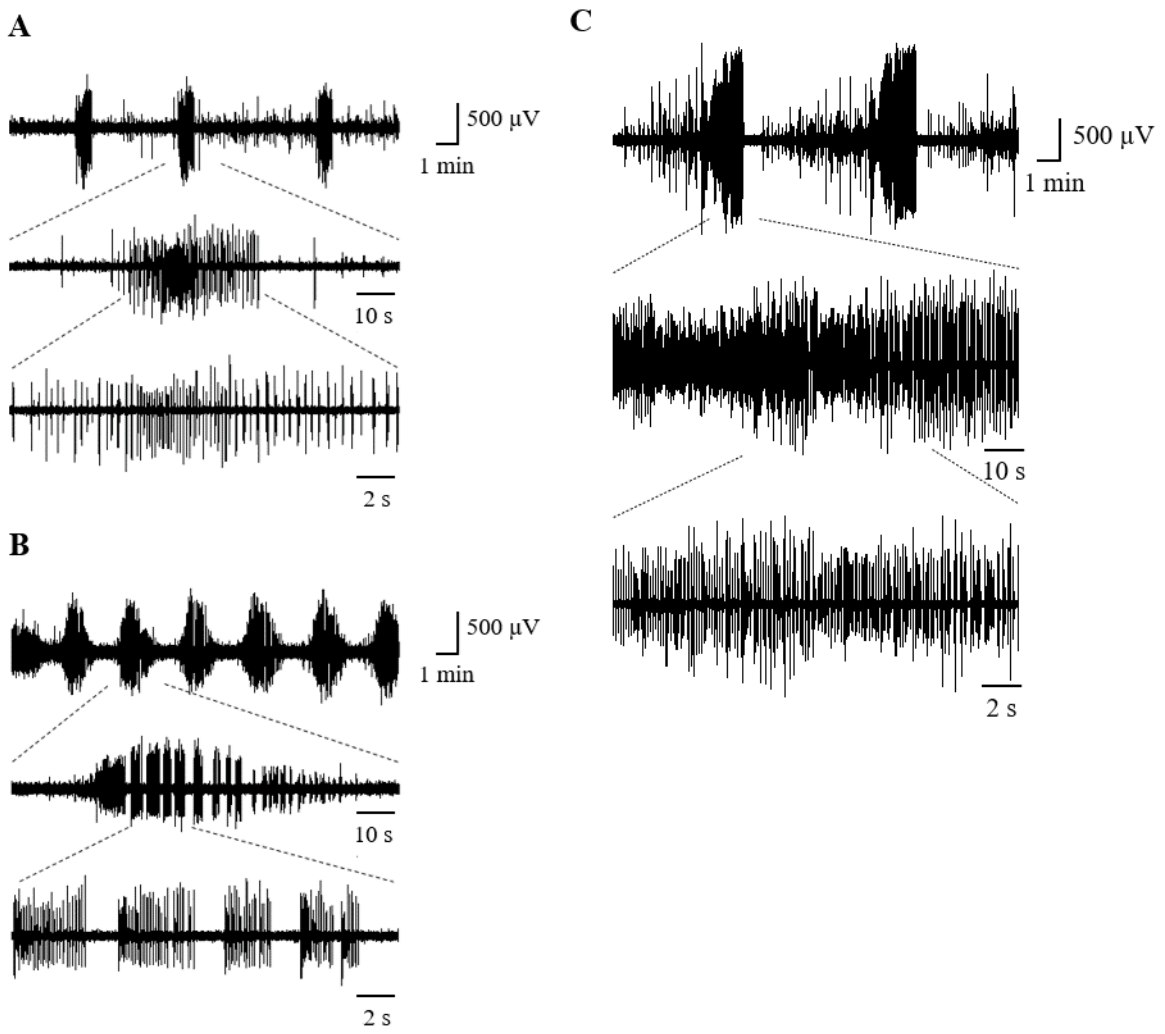

Figure 4.1: Spontaneous epileptiform activity in rhinal cortex-hippocampus organotypic slices. Representative recordings of electrographic seizure-like events in CA3 area after **(A)** 6-8 DIV, **(B)** 13-15 DIV and **(C)** 20-22 DIV. Seizure details are shown in lower traces.

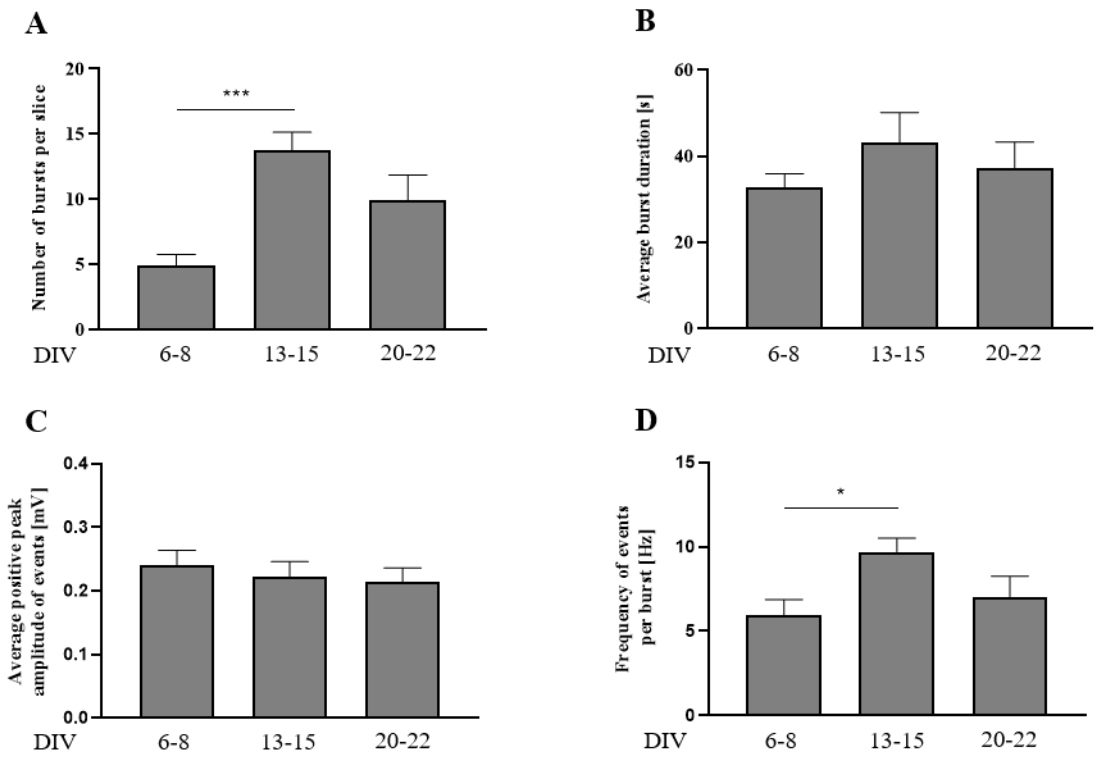

Figure 4.2: Characterization of epileptiform activity in rhinal cortex-hippocampus organotypic slices. Parameters as **(A)** number of bursts per slice, **(B)** average burst duration, **(C)** average positive peak amplitude of events and **(D)** frequency of events per burst were evaluated in slices with 6-8, 13-15 and 20-22 DIV. All values are presented as mean ± SEM. N=8-13 slices. *p<0.05, ***p<0.001, by one-way ANOVA followed by Tukey's multiple comparison test. Statistical differences are indicated by the connecting lines above the bars.

4.2. Evaluation of cell death

Cell death is one of the main characteristics of epilepsy [91], hence, a PI uptake assay was performed in EL slices, at 3, 7, 14 and 21 DIV. The fluorescence was measured separately for each region of interest, specifically DG, CA3 and CA1.

4.2.1. PI uptake

PI is not permeant to live cells, thus it is commonly used to detect dead cells in a population. PI-positive cells can be identified as bright dots in **Fig. 4.3A.** Although some PI-positive cells can be observed throughout the whole hippocampus, most of them are located in the granular and pyramidal areas, with the CA3 region being the one that incorporated less PI. PI fluorescence (**Fig. 4.3B**) vary between regions and throughout time in culture. In the DG area, values of PI fluorescence are slightly increased in relation to 3 DIV, but no significant difference was obtained. PI fluorescence in CA3 region at 7 DIV is similar to 3 DIV but depicts a significant reduction at 14 DIV (7 DIV: 124.7 ± 22.65 vs 14 DIV: 54.1 ± 16.9, * $p<0.05$) and 21 DIV (7 DIV: 124.7 ± 22.65 vs 21 DIV: 48.37 ± 13.42, * $p<0.05$). In the CA1 area PI uptake does not show significant differences compared to 3 DIV.

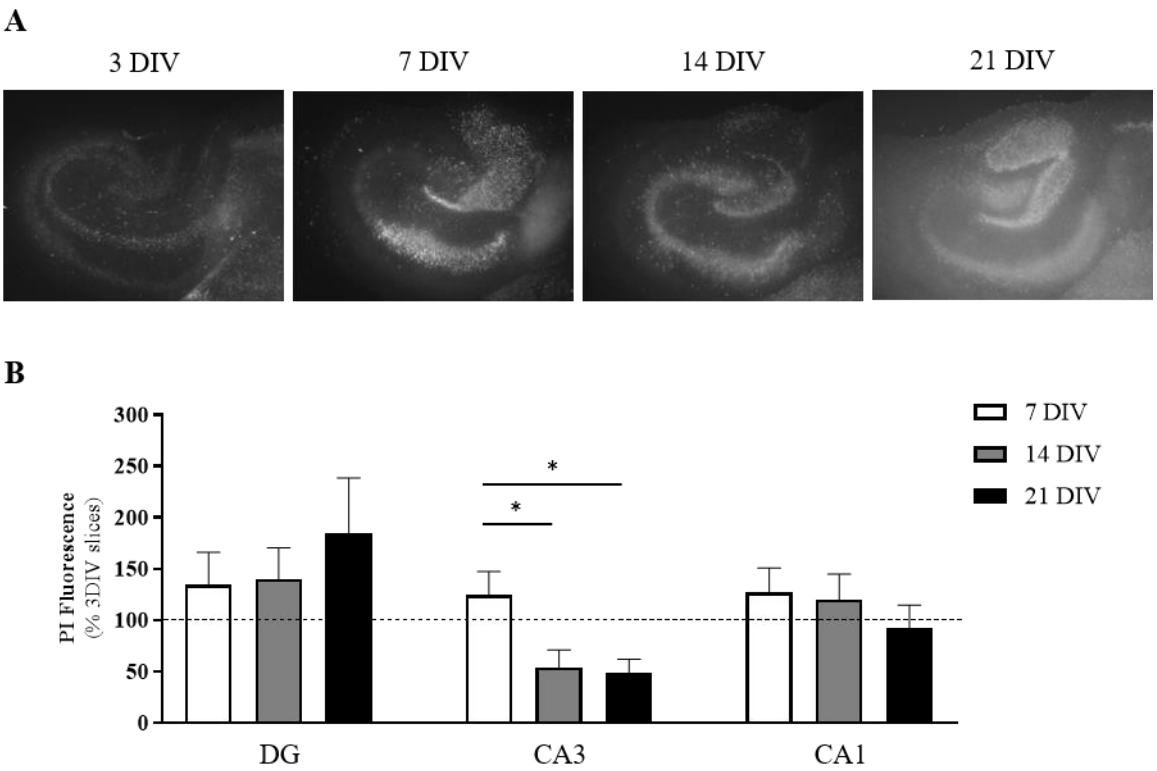

Figure 4.3: Propidium iodide uptake in rhinal cortex-hippocampus organotypic slices. (A) Representative fluorescence images of PI uptake in the hippocampus throughout time in culture. **(B)** Quantification of PI uptake was performed with ImageJ software by individualizing each hippocampal region (DG, CA3 and CA1) and is expressed as percentage of 3 DIV slices, represented by the dashed line. All values are presented as mean ± SEM. N=4-11 slices per DIV. * $p<0.05$, by one-way ANOVA followed by Tukey's multiple comparison test. Statistical tests were performed according to the connecting lines above the bars.

To fully prove that the majority of PI-positive cell were indeed neurons, a marker of mature neurons (NeuN) was applied to PI-stained slices in an immunohistochemistry assay. Confocal images (**Fig. 4.4**) confirmed the presence of PI-positive neurons in granular and pyramidal layers of the hippocampus. At 7 DIV, slices already show PI uptake by neurons (arrows in **Fig. 4.4A**). At 14 DIV, the number of PI-positive neurons is clearly increased (arrows in **Fig. 4.4B**), but at 21 DIV (**Fig. 4.4C**) only a few PI-positive neurons can be identified. Also, by analysing each area, the reduced number of damaged neurons in CA3 is obvious, while granular neurons and CA1 pyramidal neurons are heavily affected by neuronal death. Overall, we showed the occurrence of neuronal death in EL slices, with DG and CA1 being the most affected areas and CA3 the least disturbed.

4.2.2. Presence of Gasdermin D in neurons

Since PI cannot distinguish between the various types of cell death, we decided to assess the inflammatory cell death pyroptosis, nowadays known to be associated with neurological diseases [57]. Thus, an immunohistochemistry assay was performed in EL slices using antibodies against the neuronal marker NeuN and GSDMD, the effector protein in pyroptosis. As can be observed in **Fig. 4.5**, GSDMD shows co-localization with neurons ($NeuN^+/GSDMD^+$), either granular or pyramidal, but also with other cell types ($NeuN^-/GSDMD^+$) (**Annex 1**) at all time points evaluated. However, there is a clear increase in GSDMD staining from 7 DIV (**Fig. 4.5A**) to 14 DIV (**Fig. 4.5B**) and 21 DIV (**Fig. 4.5C**). CA3 area, the least affected by neuronal death as demonstrated before, also shows less presence of GSDMD than the other areas. In DG and CA1, the occurrence of GSDMD is higher, as is the PI staining, and the marker spreads itself along the borderlines of the nuclei, as pointed by the arrows in **Fig. 4.5B1a** and **Fig. 4.5C3a**, suggesting the cytoplasmatic presence of GSDMD.

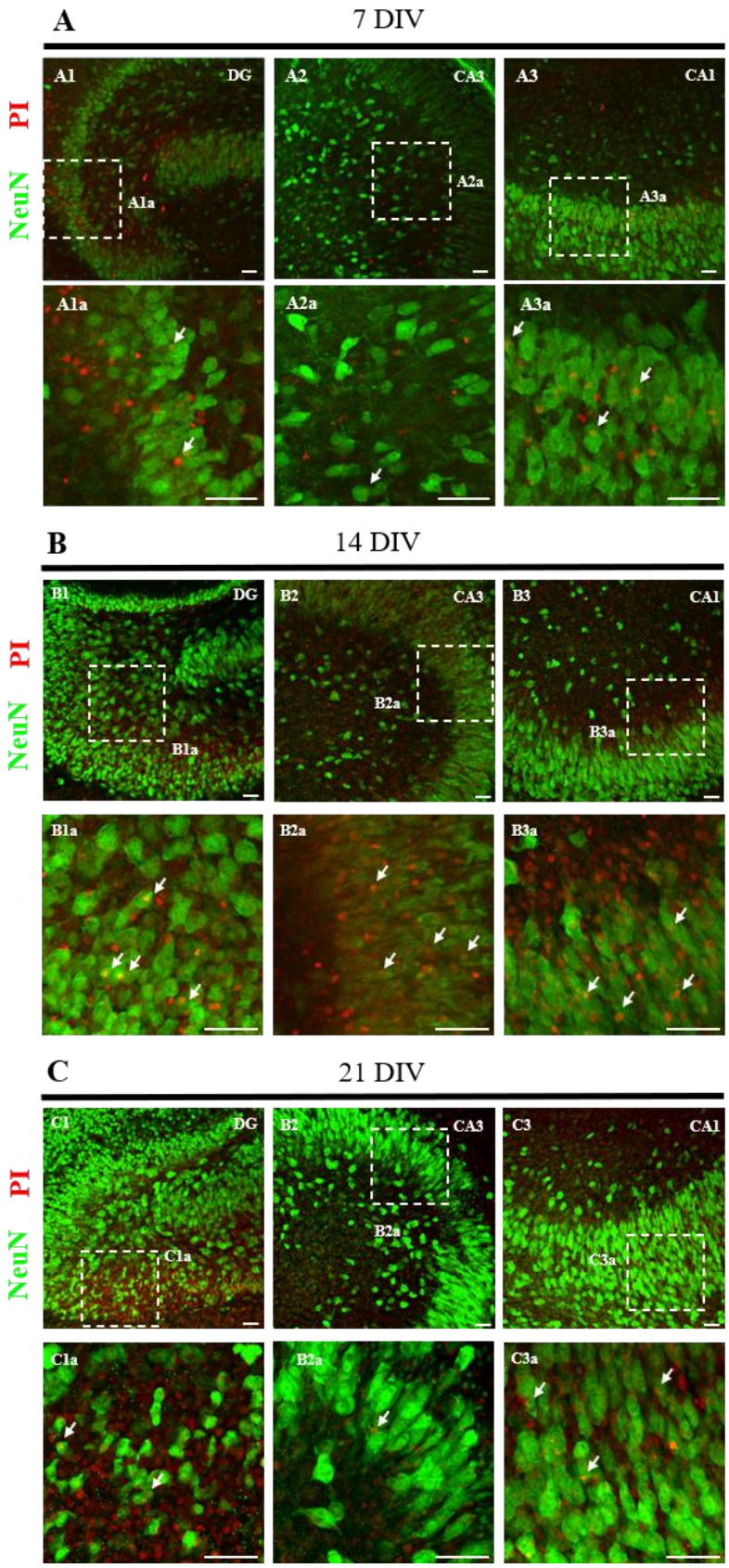

Figure 4.4: Double staining of NeuN and PI in epileptic-like rhinal cortex-hippocampus organotypic slices. Representative images of NeuN stained neurons (green) and PI-stained cells (red) at **(A)** 7 DIV, **(B)** 14 DIV and **(C)** 21 DIV, acquired on a confocal laser microscope (Zeiss LSM 710) with a 20x objective. Magnified images of the dashed areas are shown. Arrows point to PI-positive neurons (in orange). Scale-bar, 50 µm.

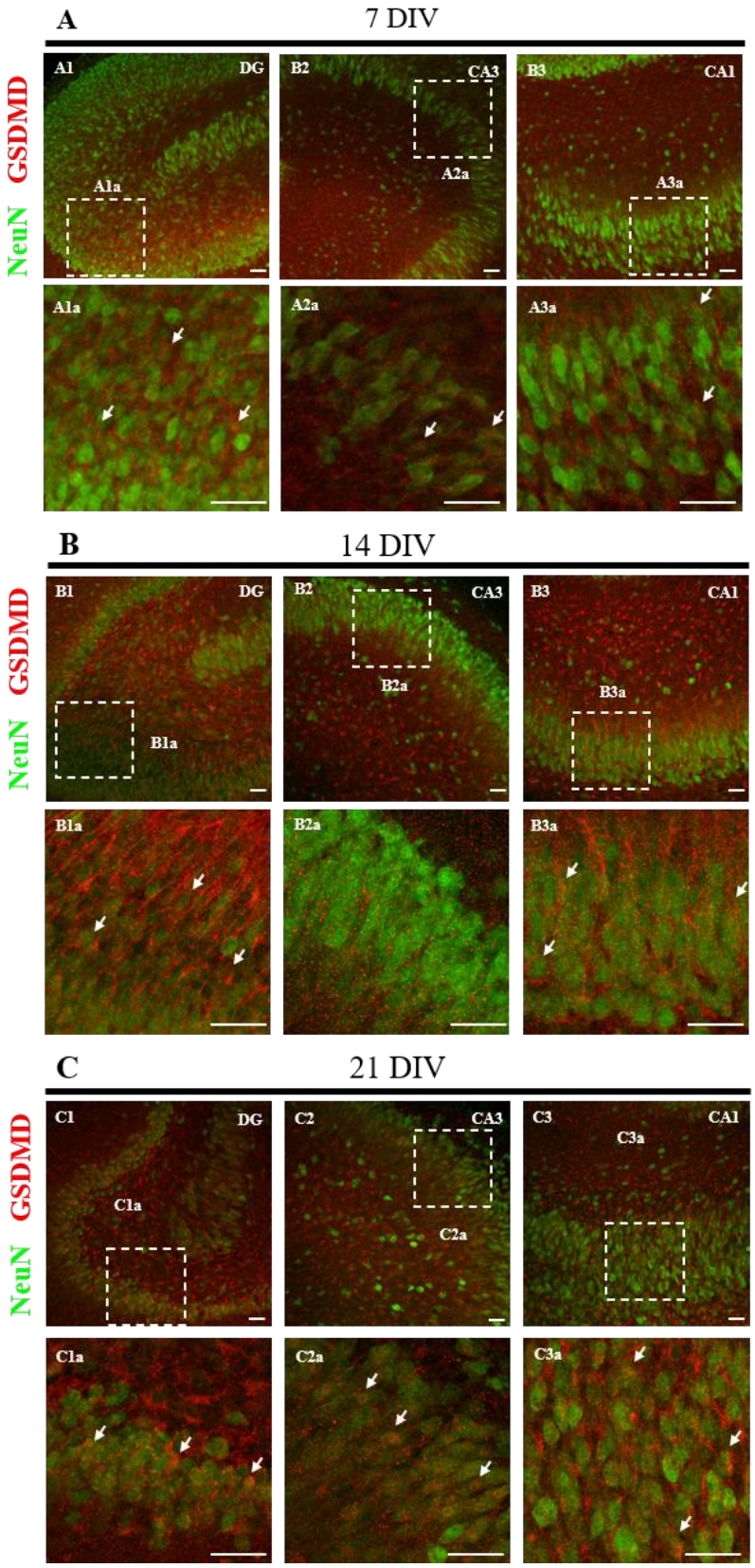

Figure 4.5: Co-localization of GSDMD with neurons in epileptic-like rhinal cortex-hippocampus organotypic slices. Representative images of NeuN stained neurons (green) and GSDMD (red) at **(A)** 7 DIV, **(B)** 14 DIV and **(C)** 21 DIV were acquired on a confocal laser microscope (Zeiss LSM 710) with a 20x objective. Magnified images of the dashed areas are shown. Arrows point to GSDMD positive neurons (in orange). Scale-bar, 50 μm.

4.2.3. Gasdermin D cleavage in the hippocampus

GSDMD is a natural occurring protein. The co-localization of GSDMD in neurons does not necessarily means neuronal death by pyroptosis since the effector protein in pyroptosis is the GSDMD-NT, released upon cleavage by inflammatory caspases.

Thus, the expression pattern of full length (FL)-GSDMD and GSDMD-NT in the hippocampus of EL slices throughout time in culture was assessed. **Fig 4.6A** shows presence of either FL-GSDMD or cleaved GSDMD-NT from 3 to 21 DIV slices. The densitometry analysis was performed and the ratio of GSDMD-NT vs FL-GSDMD was calculated (**Fig. 4.5B**). There is a significant increase in GSDMD cleavage from 3 to 7 DIV (3 DIV: 0,887 ± 0,049 vs 7 DIV: 1.178 ± 0.031, $p<0.05$). From 7 DIV onwards, this ratio decreases significantly (7 DIV: 1.178 ± 0.031 vs 14 DIV: 0.91 ± 0.083, $p< 0.05$; 7 DIV: 1.178 ± 0.031 vs 21 DIV: 0.507 ± 0.082, $p<0.001$; 14 DIV: 0.91 ± 0.08 vs 21 DIV: 0.507 ± 0.082, $p<0.01$). Previous results investigated the occurrence of necrosis by the calpain mediated cleavage of αII-Spectrin (**Annex 2**). Altogether, results showed an increase in αII-Spectrin cleavage, as GSDMD cleavage started to decrease. Nevertheless, these results prove the occurrence of cell death by pyroptosis and given the observed occurrence of GSDMD in neurons, it is plausible to hypothesise that neuronal death by pyroptosis is occurring in EL slices.

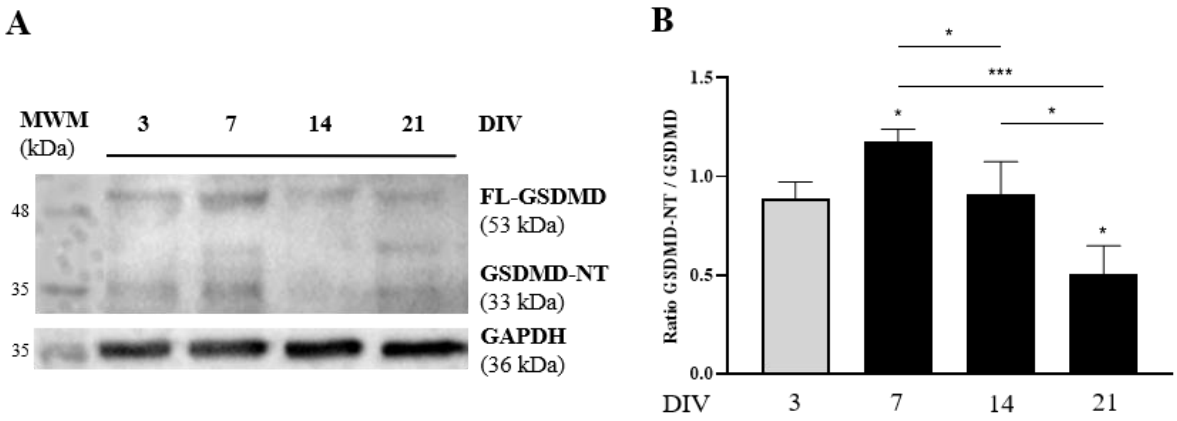

Figure 4.6: Expression pattern of GSDMD in the hippocampus of rhinal cortex-hippocampus organotypic slices. (A) Representative immunoblots for FL-GSDMD (53 kDa), GSDMD-NT (33 kDa) and GAPDH (36 kDa) at 3, 7, 14 and 21 DIV. **(B)** Densitometry analysis of FL-GSDMD and GSDMD-NT was performed with ImageJ software. Results are presented as the ratio GSDMD-NT to FL-GSDMD. All values are presented as mean ± SEM. N=3-4 independent cultures. *p<0,05, **p<0.01, ***p<0.001, by one-way ANOVA followed by Tukey's multiple comparison test. Statistical tests were performed in comparison with 3 DIV, except if otherwise indicated by the connecting lines above the bars.

4.3. Expression pattern of NLRP3 domains

GSDMD is cleaved by inflammatory caspases, namely Caspase-1. Therefore, the role of NLRP3 inflammasome in this system was addressed. For that, the overall expression pattern of NLRP3 domains was determined (**Fig. 4.7**). NLRP3 and ASC domains, as well as cleaved Caspase-1, are present in EL slices from 3 DIV onwards, as can be observed by the representative immunoblots depicted in **Fig. 4.7A**. As for NLRP3 (**Fig. 4.7B**), its expression progressively decreases over time in culture from 3 DIV on (3 DIV: 0.69 ± 0.06; 7 DIV: 0,48 ± 0,05, $p<0.05$; 14 DIV: 0.39 ± 0.05, $p<0.01$; 21 DIV 0.34 ± 0.04, $p<0.001$). ASC expression (**Fig. 4.7C**) however, has its minimum at 3 DIV, shows a tendency to increase to 7 DIV and plateaus until 21 DIV. Finally, active Caspase-1 (**Fig. 4.7D**) has a minimum at 3 DIV and depicts a tendency to increase afterwards, although without statistical significance. To note that Caspase-1 detection was not very effective and requires further optimization. Nevertheless, the presence of active Caspase-1, processed by the autoproteolytic cleavage of pro-Caspase-1, indicates NLRP3 assembly.

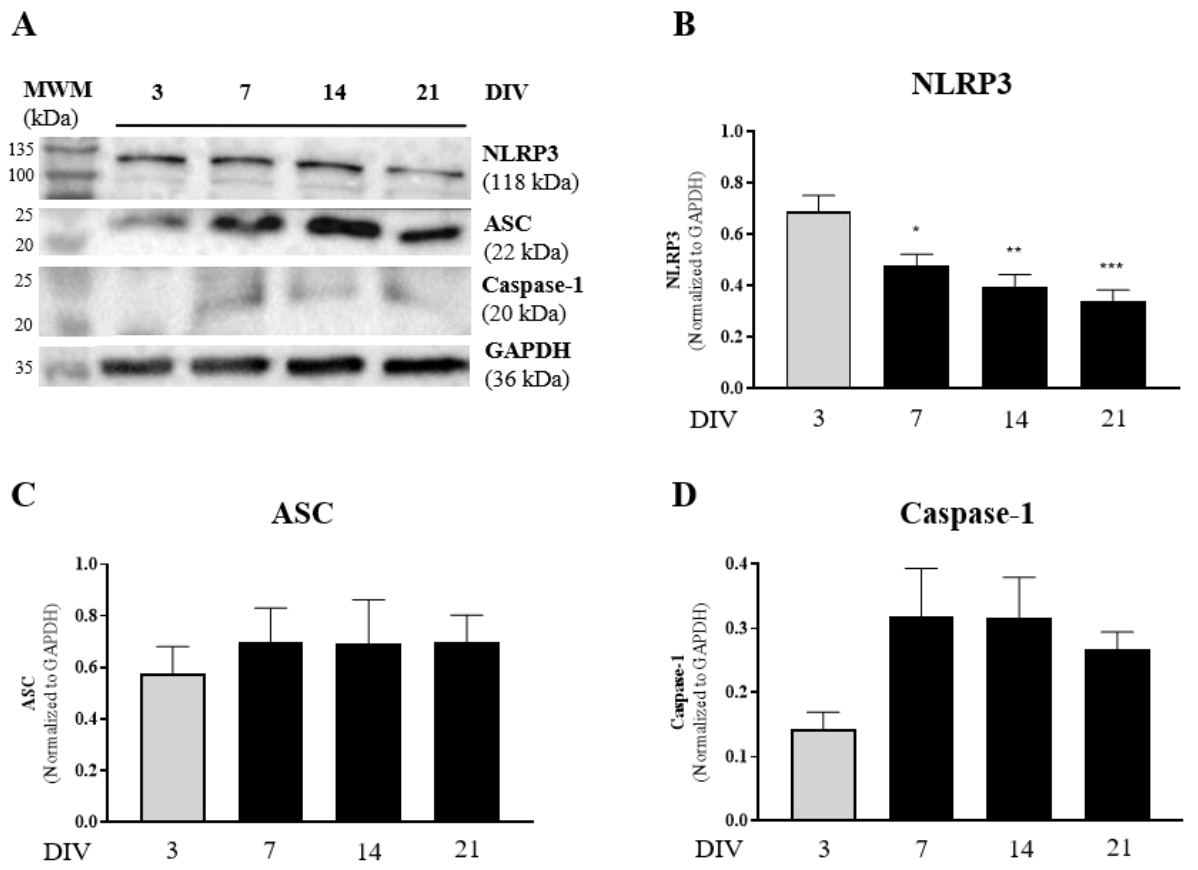

Figure 4.7: Expression pattern of NLRP3 inflammasome domains in the hippocampus of rhinal cortex-hippocampus organotypic slices. (A) Representative immunoblots for NLRP3 (118 kDa), ASC (22 kDa), Caspase-1 (20 kDa) and GAPDH (36 kDa) at 3, 7, 14 and 21 DIV. Densitometry analysis of **(B)** NLRP3 [N=9], **(C)** ASC [N=9] and **(D)** Caspase-1 [N=5] was performed with ImageJ software using GAPDH as internal control. All values are presented as mean ± SEM. **p<0.01, ***p<0.001, by one-way ANOVA followed by Tukey's multiple comparison test. Statistical tests were performed in comparison with 3 DIV.

4.4. Release of IL-1β

IL-1β is considered a pro-epileptogenic cytokine, as its exacerbated release can promote the development of epilepsy [55]. Having proved the activation of the inflammasome in EL slices, and since NLRP3 signalling is the major pathway involved in IL-1β processing, it was relevant to quantify the IL-1β released by these slices over time in culture.

As depicted in **Fig. 4.8**, IL-1β levels increase gradually from 3 DIV onwards, until it reaches statistical significance at 17 DIV (3 DIV: 18.73 ± 0.465 vs 17 DIV: 67.21 ± 13.86, p<0.01). However, from 17 DIV onwards, values are significantly reduced (20 DIV: 21.96 ± 5.133; p<0.01 and 21 DIV: 27.2 ± 3.77, p<0.01).

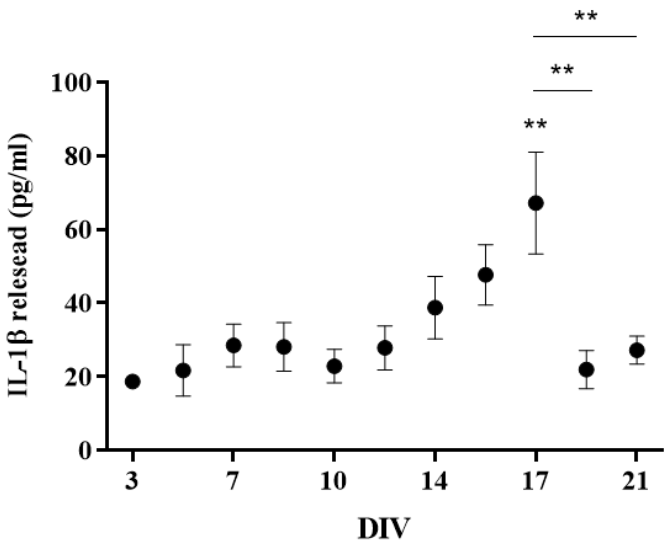

Figure 4.8: IL-1β released by epileptic-like rhinal cortex-hippocampus organotypic slices. The pro-inflammatory cytokine was quantified in culture medium collected at 3, 6, 7, 8, 10, 13, 14, 15, 17, 20 and 21 DIV by ELISA. All values are presented as mean ± SEM. N=4-7 independent cultures. ** p<0.01, by one-way ANOVA followed by Tukey's multiple comparison test. Statistical tests were performed in comparison with 3 DIV, except if otherwise indicated by the connecting lines above the bars. Quantification was performed in collaboration with Mafalda Carvalho.

4.5. Characterization of NLRP3 in neurons

With evidence of NLRP3 activation in EL slices, our next target was to characterize NLRP3 signalling in neurons. To address the presence of NLRP3 components in neurons, immunohistochemistry assays were performed, making use of antibodies against NLRP3 and ASC coupled with NeuN.

Fig. 4.9 shows expression of NLRP3 domain in granular and pyramidal neurons from 7 DIV on. At 7 DIV (**Fig. 4.9A**), NLRP3 domain is expressed in neurons across all regions of the hippocampus, with a prevalence in CA1. At 14 DIV (**Fig. 4.9B**), NLRP3 domain expression in CA1 is maintained, and it increases in DG and CA3. After 3 weeks in culture (**Fig. 4.9C**), NLRP3 expression seems to decrease in all areas. However, CA1 continues to be the one with the highest NLRP3 expression. Overall, CA3 pyramidal neurons depict the least expression of NLRP3 at any timepoint, and CA1 pyramidal neurons shows the largest amount of NLRP3 at 14 DIV, reducing slightly to 21 DIV.

Confocal images of ASC paired with NeuN (**Fig 4.10**) shows co-localization in 7, 14 and 21 DIV slices. From 7 (**Fig. 4.10A**) to 14 DIV (**Fig. 4.10B**), ASC-positive neurons increase in CA3 and CA1, however, no alterations were found in DG. At 21 DIV slices (**Fig. 4.10C**), ASC expression in pyramidal neurons decreases slightly (**Fig. 4.10C2 and 4.10C3**) and in granular neurons increases (**Fig. 4.10C1**) from 14 DIV. Altogether, ASC expression in granular and pyramidal neurons increases on our model of epileptogenesis. **Table 1** summarizes the expression levels of NLRP3 domain and ASC in granular and pyramidal neurons of EL slices.

Table 4.1: Expression levels of NLRP3 domain and ASC in granular and pyramidal neurons of epileptic-like rhinal cortex-hippocampus organotypic slices. +++, high expression; ++, moderate expression; +, low expression.

DIV	NLRP3			ASC		
	DG	CA3	CA1	DG	CA3	CA1
7	+	+	+++	+	+	+
14	++	++	+++	+	++	++
21	+	+	++	+++	++	++

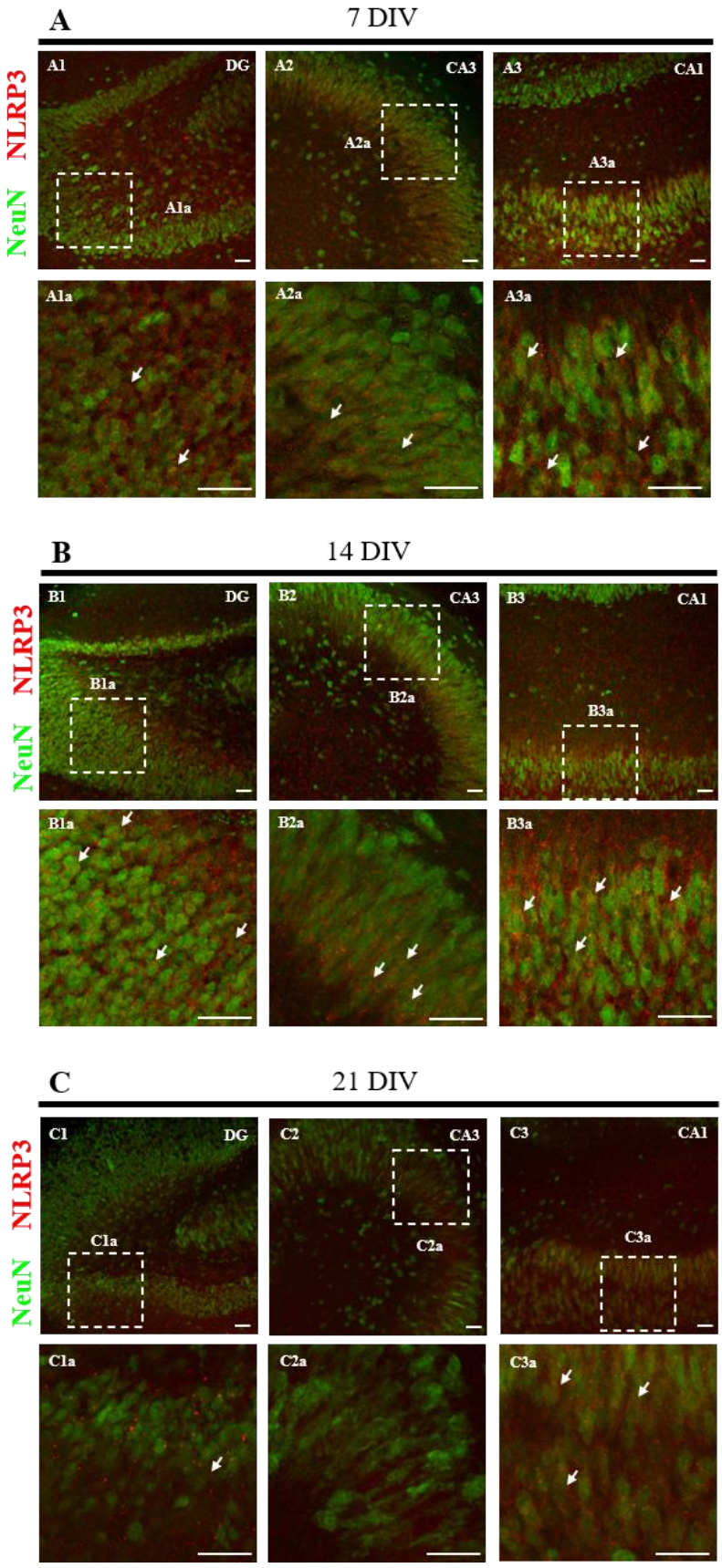

Figure 4.9: Co-localization of NLRP3 domain with neurons in rhinal cortex-hippocampus organotypic slices. Representatives images of NeuN stained neurons (green) and NLRP3 domain (red) at **(A)** 7 DIV, **(B)** 14 DIV and **(C)** 21 DIV, acquired on a confocal laser microscope (Zeiss LSM 710) with a 20x objective. Magnified images of the dashed areas are shown. Arrows point to co-localization of NLRP3 domain with neurons (in orange) Scale-bar, 50 µm.

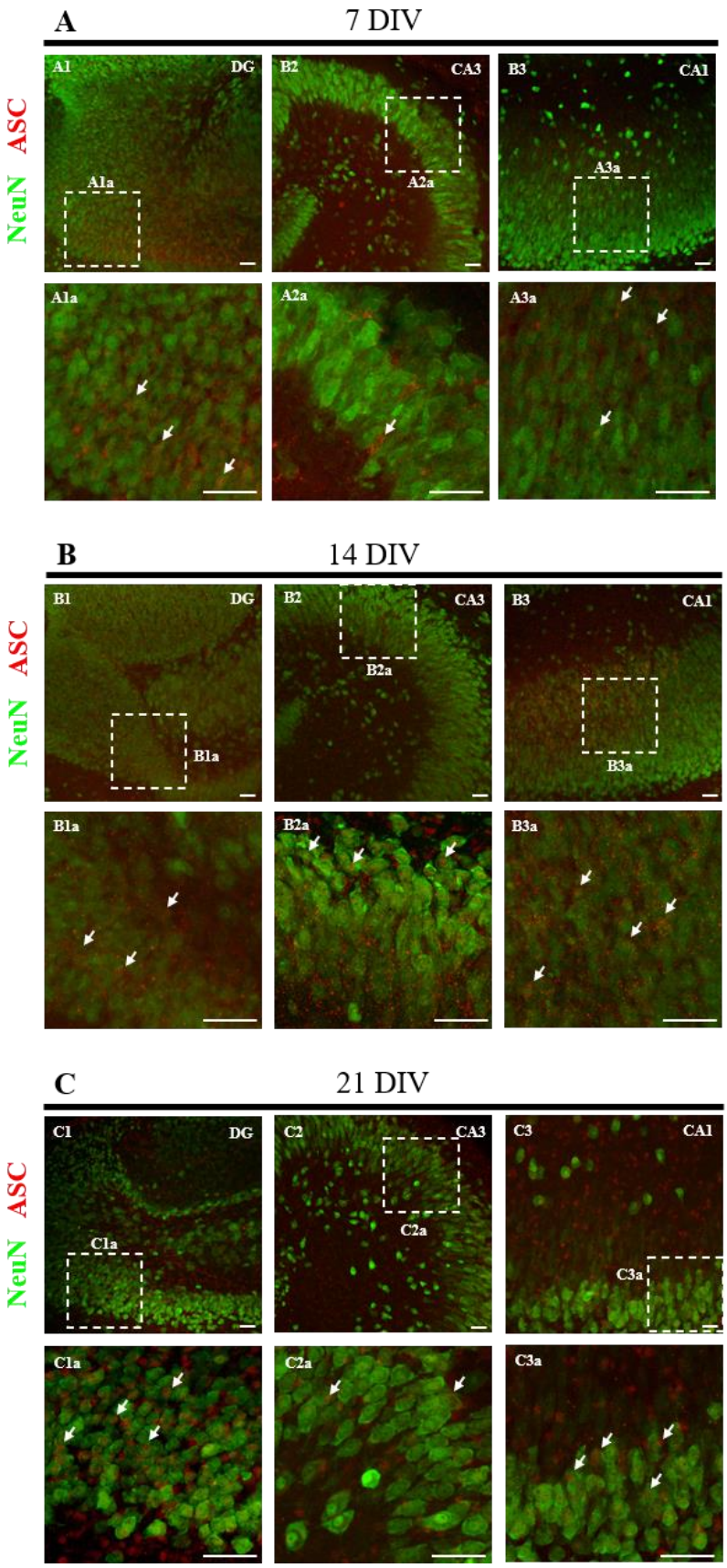

Figure 4.10: Co-localization of ASC with neurons in rhinal cortex-hippocampus organotypic slices. Representatives images of NeuN stained neurons (green) and ASC (red) at **(A)** 7 DIV, **(B)** 14 DIV and **(C)** 21 DIV, acquired on a confocal laser microscope (Zeiss LSM 710) with a 20x objective. Magnified images of the dashed areas are shown. Arrows point to co-localization of ASC with neurons (in orange) Scale-bar, 50 µm.

4.6. ROS as a potencial NLRP3 activator

In the previous sections we proved that NLRP3 domains are present in EL slices. Moreover, IL-1β release and GSDMD cleavage are dependent on NLRP3/Caspase-1 axis and thus it's plausible to propose that NLRP3 is activated in this system. EL slices undergo a gradual removal of serum from the culture medium [37]. Serum deprivation-induced ROS production was described in other systems [129], and we decided to evaluate if ROS could be a potential NLRP3 activator in our model. For that, ROS production was indirectly evaluated in the hippocampus through DCF fluorescence (see section 3.4). DCF fluorescence images were acquired at 3, 7, 14, 21 DIV and fluorescence intensities were quantified through ImageJ software (**Fig. 4.11**).

There was an increase in DCF fluorescence from 3 DIV to 7 DIV, but no more visual differences were perceptible in **Fig. 4.11A.** DCF fluorescence in DG **(Fig. 4.11B**) showed a significant increase from 3 DIV slices (100 ± 9.42) to 14 and 21 DIV slices (14 DIV: 320 ± 42.2, $p<0.0001$; 21 DIV: 346.6 ± 56.76, $p<0.0001$). DCF fluorescence is also significantly different between 7 DIV and 21 DIV slices (7 DIV: 204.8 ± 20.26; 21 DIV: 346.6 ± 56.76, $p<0.05$). In the CA3 area (**Fig. 4.11C**), DCF fluorescence increases significantly from all time points up to 21 DIV slices (3 DIV: 100 ± 5.96 vs 7 DIV: 143.6 ± 21.09, $p<0.01$; 3 DIV vs 14 DIV: 153 ± 22.8, $p<0.01$ and 3 DIV vs 21 DIV: 288.9 ± 46.37, $p<0.0001$). Finally, in the CA1 (**Fig. 13D**), ROS production augments significantly from 3 DIV slices (100 ± 8.46) and plateaus at similar levels from 7 to 21 DIV slices (3 DIV vs 7 DIV: 268.4 ± 33.96, $p<0.0001$; 3 DIV vs 14 DIV 231.4 ± 28.86, $p<0.01$ and 3 DIV vs 21 DIV 241 ± 30.3, $p<0.001$). Altogether, this data shows that ROS production rises with time in culture and can act as a NLRP3 activator. However, this hypothesis was not explored in this study.

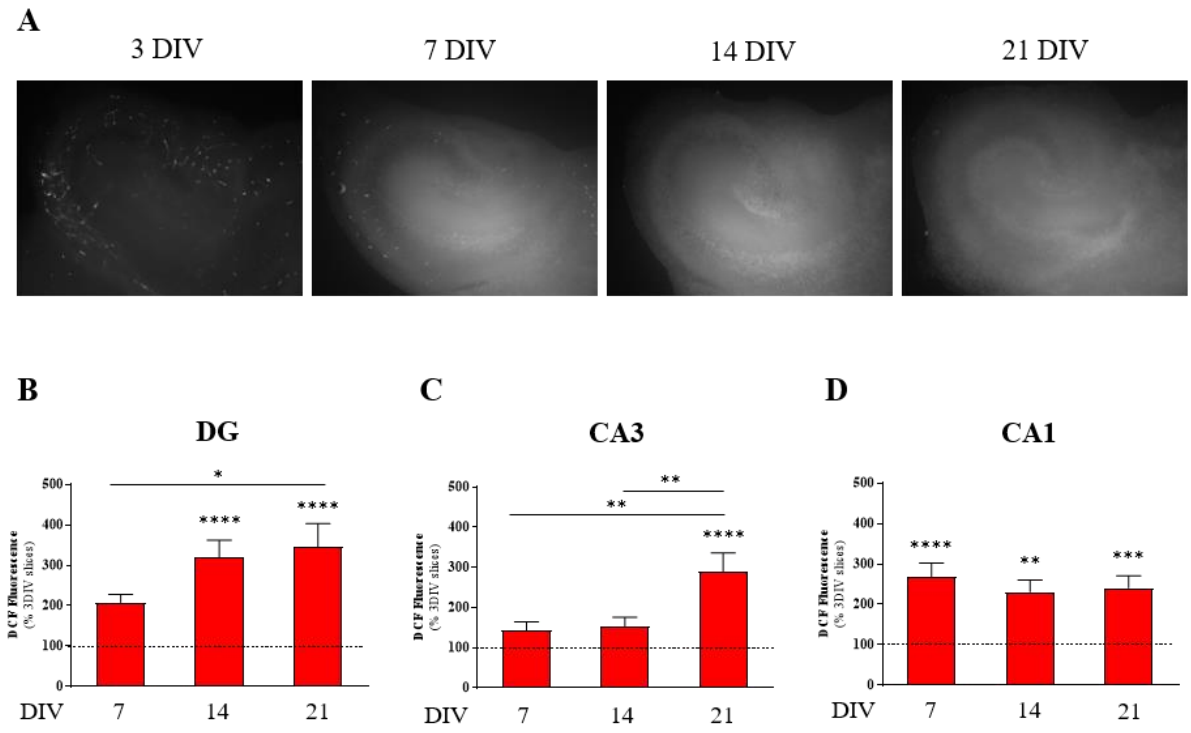

Figure 4.11: DCF fluorescence in rhinal cortex-hippocampus organotypic slices. (A) Representative imagens of DCF fluorescence, proportional to ROS production, throughout time in culture. Quantification of DCF fluorescence in **(B)** DG, **(C)** CA3 and **(D)** CA1 was performed in ImageJ software by individualizing each hippocampal region and is expressed as percentage of 3 DIV slices, represented by the dashed lines. All values are presented as mean ± SEM. N=12-24 slices. *p<0.05, **p<0.01, ***p<0.001, ****p<0.0001, by one-way ANOVA followed by Tukey's test. Statistical tests were performed in comparison with 3 DIV, except if otherwise indicated by the connecting lines above the bars.

4.7. NLRP3 inhibition by MCC950 - Impact in spontaneous epileptiform activity

Epileptic-like rhinal cortex-hippocampus slices depict spontaneous epileptiform activity throughout time in culture. Therefore, these slices were used to evaluate the impact of MCC950, a selective NLRP3 inflammasome inhibitor, in the development of epileptiform activity. As explained in section 3.11, in these experiments 13-15 DIV slices were recorded in NBA medium for 30 min. After 30 min with ictal-like activity, the superfused medium was changed to NBA with freshly added MCC950 (1µM and 5µM), and the recording proceeded for 1 h more.

Fig 4.12A, represents a recording of a 14 DIV slice in which the perfused medium was supplemented with 1µM MCC950. Visually, the activity that started as mainly ictal discharges, was almost nullified after the addition of MCC950, with the effect being very fast. As MCC950 is a compound diluted in DMSO, a solvent usually prejudicial to living tissue [130], a recording was performed where at the perfused medium was added 0.01% DMSO (equivalent to the amount present in 1µM MCC950). In this experiment (**Fig. 4.12B**), the spontaneous activity was preserved, as ictal discharges, indicating that this concentration of DMSO does not interfere with our system. A couple of experiments were performed in the presence of 5µM MCC950, and the equivalent 0.05% DMSO, to check if it would cease the activity faster. Such did not occur (**Annex 3**) and since the effect of MCC950 was positive at a lower concentration, with reduced side effects in a pharmacological point of view, MCC950 at 1µM was used in this work.

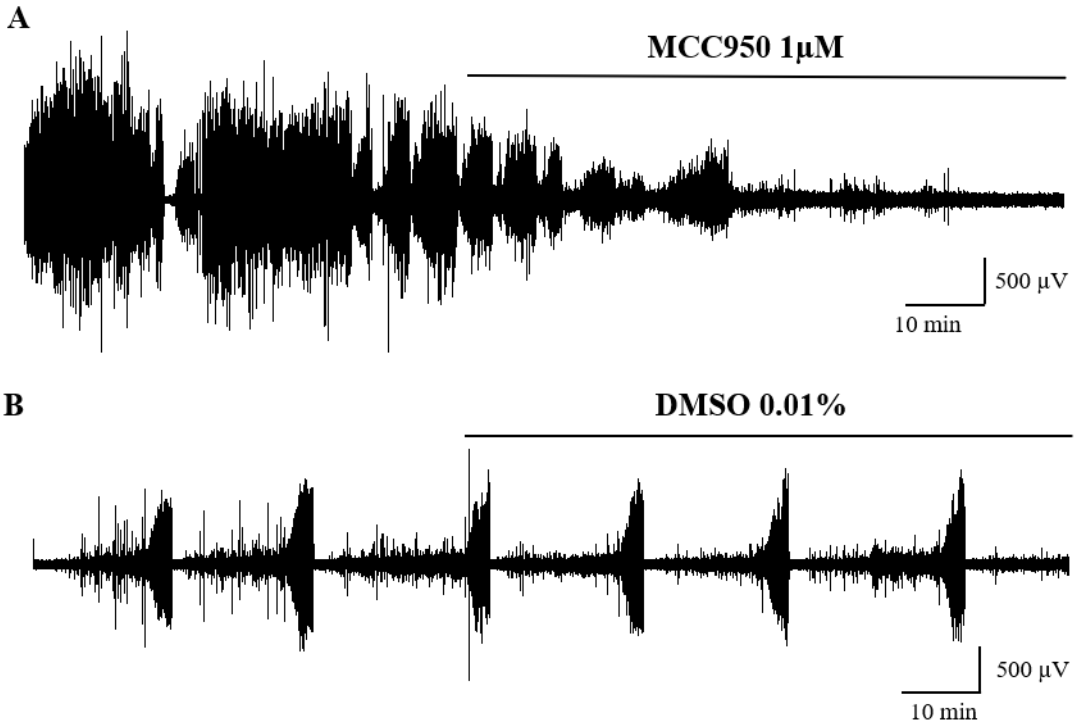

Figure 4.12: Impact of MCC950 on the epileptiform activity depicted by rhinal cortex-hippocampus organotypic slices. Representative recordings of electrographic seizure-like events in CA3 in slices with 13-15 DIV. Slices were exposed to **(A)** 1µM MCC950 and **(B)** 0,01% DMSO after 30 min of recording.

The data was analysed in the first 30 min and for 30 more min after 10 min of MCC950 addition, considering the parameters already mentioned (see section 3.10). MCC950 significantly reduced the number of bursts (**Fig. 4.13A**) (13 ± 2.08 vs 5.42 ± 1.6, $p<0.01$), the average positive peak amplitude (**Fig. 4.13C**) (0.28 ± 0.03 vs 0.17 ± 0.03, $p<0.05$) and the frequency of events (**Fig. 4.13D**) (7.12 ± 1.16 vs 3.79 ± 0.76, $p<0.05$). The average burst duration (**Fig. 4.13B**) shows a tendency for decrease, but

with no statistical significance. Overall, these results indicate a strong impact of NLRP3 inhibition in the reduction of spontaneous epileptiform activity.

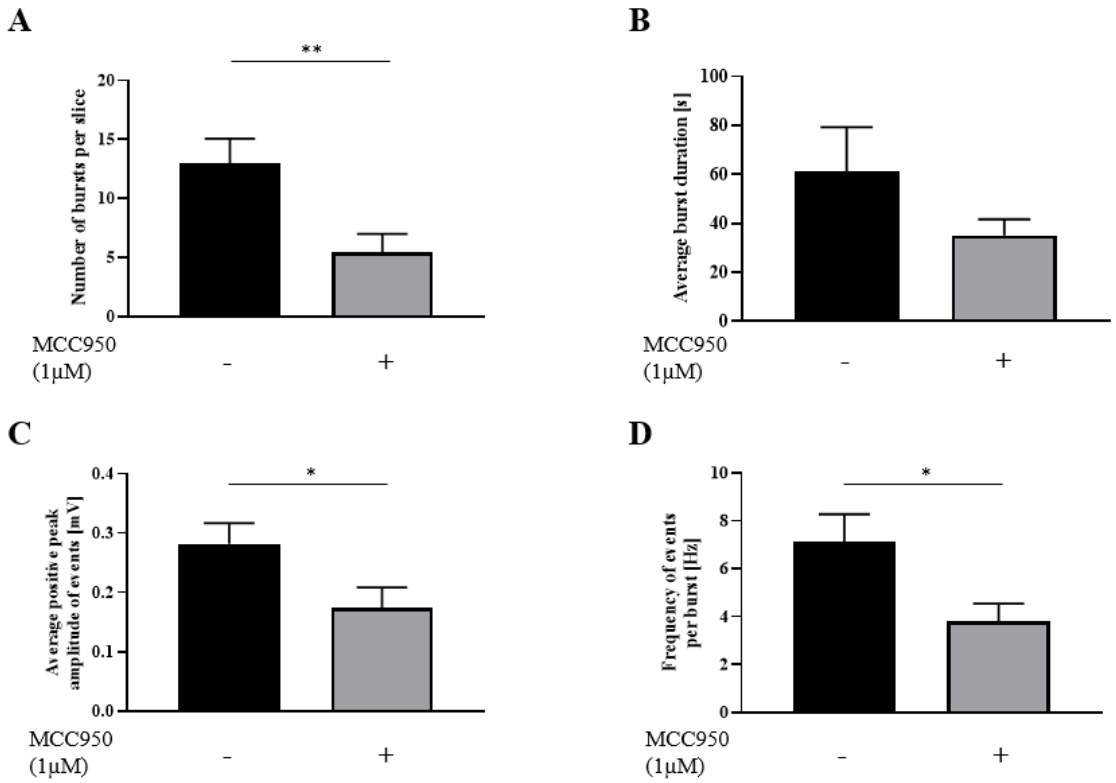

Figure 4.13: Impact of MCC950 on the parameters of the epileptiform activity depicted by rhinal cortex-hippocampus organotypic slices. Slices were exposed to 1µM MCC950 after 30 min of recording. The parameters evaluated were **(A)** number of bursts per slice, **(B)** average burst duration, **(C)** average positive peak amplitude of events and **(D)** frequency of events per burst. All values are presented as mean ± SEM. N=12-13 slices. *p<0.05, **p<0.01, by unpaired t-test analysis. Statistical tests were performed according to the connecting lines above the bars.

5. Discussion

In this study, we aimed to assess NLRP3-mediated cell death by pyroptosis and the inflammasome inhibition effect in epileptiform activity. We show that the progression of epileptiform activity is accompanied by expression of NLRP3 inflammasome and markers of cellular death, namely PI and, the recently discovered, pyroptosis-associated protein GSDMD [131] in granular and pyramidal neurons. We also show variations in the release of the pro-inflammatory cytokine IL-1β and in ROS production. Finally, the selective inhibition of the NLRP3 inflammasome activation, by MCC950, has a positive impact in halting epileptiform activity.

5.1. Characterization of spontaneous epileptiform activity

As previously proven, in hippocampal slices, epileptiform activity evolves from interictal, to major ictal-like discharges as time in culture progresses [32]. This works confirms the development of epileptiform activity in rhinal-cortex hippocampal organotypic slices from 6-8 DIV, where slices already present mixed-interictal and ictal-like activity (**Fig. 4.1A**). This activity evolves, to major ictal activity from 13-15 DIV onwards, earlier than Dyhrfjeld and colleagues described [32], suggesting that triggering factors of seizure generation, like neuroinflammation, sprouting and pro-inflammatory cytokine release, namely IL-1β, are appearing sooner in our model. IL-1β was considered to be related with epilepsy progression several years ago [55], and microglia is the main contributor to its production [132]. Therefore, we also measured the levels of released IL-1β in our system and values increased significantly until 17 DIV

reducing to 20-22 DIV (**Fig 4.8**). IL-1β release was also quantified in slices maintained in the presence of serum throughout all culture time. These slices do not depict epileptiform activity and the IL-1β released was so low that could not be quantified until 14 DIV. After 14 DIV values remained extremely low in comparison with the same time points in EL slices (**Annex 4**). Moreover, results from my colleague Mafalda Carvalho project (**Annex 5**) show an intensification in Iba-1^{+}/CD68^{+} amoeboid M1 microglia presence in EL slices at 14 and 21 DIV. M1 microglia is known to contribute to the propagation of inflammation by releasing pro-inflammatory cytokines like IL-1β [133], which can be coupled with the worsening of epileptiform activity to ictal like discharges from 13-15 DIV. The characterization of epileptiform activity was based in several parameters (see section 3.10) that show signs of upsurge to 13-15 DIV slices.

5.2. Neuronal death is a key feature in this model of epileptogenesis

In epilepsy, seizures can cause damage to the brain, namely neuronal death in susceptible areas of the brain like the hippocampus [128]. The cascade of events leading to the death of neurons starts in excessive triggering of excitatory synapses, that can't be counteracted, since inhibitory GABAergic neurons are lessened [134], leading to activation of cytosolic proteases, like caspases and calpains that culminates in neuronal death [101,135]. In this study, we observed a majority of PI uptake in the DG granular and CA1 pyramidal cell layers, suggesting that neurons are not equally affected by cell death in the hippocampus. We also saw a decrease in PI positive neurons in the CA3 that goes in accordance with the literature [17]. In MTLE patients, CA1 is the most affected area by cellular death [90], in our model, it is accompanied by DG as the most affected areas regarding cellular death. All areas showed major neuronal death at 3 DIV, that can be explained by the stress caused from tissue slicing. This mechanical disruption, induces sprouting, that facilitates the incidence of hyperexcitability and leads to neuronal death [15]. However, the progression of neuronal death is not consistent, only showing significant decrease in the CA3 (**Fig. 4.3**), in accordance with it being the least affect area. This is probably due to the low number of experiments that needs to be amplified. In this study, we aimed at exploring the occurrence of neuronal death by pyroptosis by identifying the presence of the pore forming protein GSDMD. A quick analysis by western blot showed cleavage of the protein, peaking at 7 DIV (**Fig. 4.6**). Through the rest of the time in culture, GSDMD cleavage decreased, corroborating the decreased values of neuronal death in the pyramidal layers of the hippocampus (**Fig. 4.3B**). We also describe presence of GSDMD mainly in DG and CA1 neurons (**Fig. 4.5**) further confirming the incidence of neuronal death in those areas. As neuronal death kept occurring past 14 DIV, but GSDMD cleavage decreased, we ought to analyse what kind of cell death kept happening. Previous reports in our lab showed the occurrence of cell death by necrosis, throughout time in culture, via the calpain-mediated cleavage of αII-spectrin into spectrin breakdown products (SBDP) [135]. These results showed a gradual increase in αII-spectrin cleavage into SBDB 145/150 climaxing at 21 DIV (**Annex 2**). Also, no SBDP 120 was detected, confirming the hypothesis that there is no apoptosis occurring in our model [135]. Altogether, these findings suggest that, in this model of epileptogenesis in organotypic slices, neuronal death is occurring mostly by necrosis and pyroptosis.

5.3. NLRP3 inflammasome shows signs of reduction in the hippocampus

In this study, we observed a maximum of NLRP3 domain expression at 3 DIV, which indicates a priming stimulus very early in culture. Considering the massive damage caused by tissue slicing, one might hypothesise that the TNF-α released by damaged neurons is enough to induce NF-κB activation and promote synthesis of NLRP3 and pro-IL-1β. After this first stimulus, a significant decrease in NLRP3 domain was detected by western blot, at 14 and 21 DIV (**Fig. 4.7B**). However, although with lower levels of NLRP3 domain, it is possible to observe NLRP3 activation throughout culture time. Indeed, Caspase-1 expression at 7 DIV shows a tendency for increased expression in relation to 3 DIV **(Fig. 4.7D**), which goes in accordance with a small peak obtained in IL-1β released (**Fig. 4.8**). These results

match with the tendency to pyroptosis to cease throughout time in culture, as this method is dependent of NLRP3 activation and GSDMD cleavage by Caspase-1.

5.4. Granular and pyramidal neurons express NLRP3 inflammasome

Previous studies, proved the presence of NLRP3 in neurons in the spinal cord and the thalamus [76,77], but NLRP3 expression in neurons in the hippocampus is still poorly described. In immunohistochemistry assays performed with NeuN and NLRP3 domain double-pairing (**Fig. 4.9**), co-localization of NLRP3 in neurons was evident. In a more careful analysis, we can observe a higher prevalence of NLRP3 domain in the DG and CA1 areas, supporting the predominant neuronal death by pyroptosis in those areas.

All results point to a decrease in either neuronal death, GSDMD cleavage, NLRP3 expression and IL-1β release in 21 DIV slices, although, ROS production tends to increase. Previous work has shown that in primary hippocampal neurons, senescence started to occur with the extension of culture time [136]. This is mainly due to ROS mediated oxidative stress, which corroborates our result. Another alternative is that the NLRP3 domain is being released into the medium, as it is from macrophages, as a danger signal, amplifying the inflammatory response [137].

5.5. ROS production increases over time in culture

ROS are molecules produced mainly by mitochondria during ATP production. In physiological conditions, excessive levels of ROS are counteracted by antioxidant systems, ensuring homeostasis. ROS expression is modulated by the mitochondrial ROS modulator 1 (Romo1) and enhanced by oxidative stress situations [129]. Also, there are reports describing that serum deprivation causes increased ROS production [129]. This paper's findings are confirmed in our model of epileptogenesis in which slices undergo a gradual serum deprivation. We found that at 7 DIV (4-days post serum reduction), slices already show an increase in ROS production from 3 DIV, even significant in CA1 cell layer (**Fig. 4.11D**). In the DG (**Fig. 4.11B**), ROS values appear to increase to 14 DIV and further to 21 DIV, suggesting that the inflammasome is being thoroughly activated in those areas. At 21 DIV alone, ROS production is high through the whole hippocampus. These results are bolstered by my colleague's work, in which a substantial growth in Iba-1^{+}/$CD68^{+}$ amoeboid M1 microglia to 21 DIV is observed (**Annex 5**) and, as previously described, amoeboid microglia can contribute to the production of ROS, as well as IL-1β [132,133]. Although, as we showed, the expression of the NLRP3 domain tends to diminish, reaching a minimum at 21 DIV. ROS production increases the whole time in culture and is able to promote the oligomerization and activation of the inflammasome. Nevertheless, these results are preliminary and require further investigation.

5.6. NLRP3 inhibition by MCC950 has a positive effect in seizure reduction

As exposed before, NLRP3 inflammasome has the ability to process IL-1β in a Caspase-1 mediated way and, as such, is implicated in the development of spontaneous recurrent seizures [48]. It was reported that NLRP3 or Caspase-1 knockdown decreased IL-1β levels and silenced the enhancement of recurrent seizures in a SE model, being proposed that NLRP3 was key in the development of the epileptogenic process [120].

Therefore, in this study, we used MCC950 (1μM), a selective inhibitor of the NLRP3 inflammasome activation, and evaluated its effect in epileptiform activity. The recordings show an immediate reduction of ictal activity when MCC950 is added to the recording system (**Fig. 4.12A**). The data analysed confirms the weakening of spontaneous activity, with the significant lessening of number of bursts,

positive peak amplitude and frequency of events (**Fig. 4.13A, C, D**). Burst duration does not show statistical significance, but it indicates a tendency to reduce as well in the presence of MCC950 (**Fig. 4.13B**). MCC950 stock solution was prepared in DMSO, a compound usually prejudicial to this culture systems [130]. However, the deleterious effects typically caused by DMSO did not have any effect on spontaneous discharges, as a recording with only DMSO (0.01%) did not impact activity (**Fig. 4.12B**).

Overall, these are promising results, as they confirm a role of NLRP3 inflammasome signalling in the generation of spontaneous epileptiform activity. Its inhibition, by MCC950, can be a potential therapeutic target to help cease the incidence of recurrent epileptic seizures and thus, to help improve the life quality of patients with epilepsy. However, there is still the need to further test this hypothesis, as these are only preliminary results, as well as testing the impact of MCC950 in *in vivo* animal models of epilepsy that better resemble epilepsy incidence in humans.

6. Conclusions and Future Perspectives

The results obtained in this project further demonstrate the accuracy of this model on recreating the *in vivo* characteristics of epilepsy and the capability to serve as a method to develop therapies [37]. We reveal that neurodegeneration is a key factor in the epileptogenic process. This process is mainly NLRP3 driven, as this inflammasome plays a critical role in the development of epileptic-like events in rhinal cortex-hippocampus organotypic slices. NLRP3 inflammasome domains expression is coupled with increased levels of IL-1β, ROS and markers of cellular death in neurons. Among these, the pyroptosis executer protein GDSMD, as well as inflammasome components, were detected in neurons, indicating that NLRP3 mediates pyroptotic neuronal death in the hippocampus. This study also provides further proof that NLRP3 inflammasome plays an important role in the generation of spontaneous epileptiform activity, as its inhibition by MCC950 almost nullifies such activity.

Further studies should aim to clarify the inflammasome inhibition impact on neurodegeneration and IL-1β release. Also, it would be interesting to transpose these findings to an animal model of epilepsy, such as the kainate or kindling models, to provide additional evidence of MCC950 effectiveness. Furthermore, NLRP3 inflammasome targeting can bring the scientific community one step closer to a greater understanding regarding epileptogenesis and ictogenesis.

7. References

1. Fisher, R. S. *et al.* ILAE Official Report: A practical clinical definition of epilepsy. *Epilepsia* **55**, 475–482 (2014).
2. Scheffer, I. E. *et al.* ILAE classification of the epilepsies: Position paper of the ILAE Commission for Classification and Terminology. *Epilepsia* **58**, 512–521 (2017).
3. Beghi, E. The Epidemiology of Epilepsy. *Neuroepidemiology* **54**, 185–191 (2020).
4. Diederich, N. J., Moore, C. G., Leurgans, S. E., Chmura, T. A. & Goetz, C. G. Parkinson Disease With Old-Age Onset. *Arch. Neurol.* **60**, 529 (2003).
5. Cloyd, J. *et al.* Epidemiological and medical aspects of epilepsy in the elderly. *Epilepsy Res.* **68**, 39–48 (2006).
6. Niccoli, T. & Partridge, L. Ageing as a risk factor for disease. *Curr. Biol.* **22**, R741–R752 (2012).
7. Theodore, W. H. *et al.* Epilepsy in North America a report prepared under the auspices of the Global Campaign against Epilepsy, the International Bureau for Epilepsy, the International League Against Epilepsy, and the World Health Organization. *Epilepsia* **47**, 1700–1722 (2006).
8. Banerjee, P. N., Filippi, D. & Allen Hauser, W. The descriptive epidemiology of epilepsy-A review. *Epilepsy Res.* **85**, 31–45 (2009).
9. Broadbent, N. J., Squire, L. R. & Clark, R. E. Spatial memory, recognition memory, and the

hippocampus. *Proc. Natl. Acad. Sci. U. S. A.* **101**, 14515–14520 (2004).

10. Nakahara, S. *et al.* Hippocampal Pathophysiology: Commonality Shared by Temporal Lobe Epilepsy and Psychiatric Disorders. *Neurosci. J.* **2018**, 1–9 (2018).

11. Annegers, J. F. & Coan, S. P. The risks of epilepsy after traumatic brain injury. *Seizure* **9**, 453–457 (2000).

12. Norwood, B. A. *et al.* Classic hippocampal sclerosis and hippocampalonset epilepsy produced by a single ́cryptić episode of focal hippocampal excitation in awake rats. *J. Comp. Neurol.* **518**, 3381–3407 (2010).

13. Lewis, D. V. Losing neurons: Selective vulnerability and mesial temporal sclerosis. *Epilepsia* **46**, 39–44 (2005).

14. Seress, L. *et al.* Survival of mossy cells of the hippocampal dentate gyrus in humans with mesial temporal lobe epilepsy. *J. Neurosurg.* **111**, 1237–1247 (2009).

15. Scharfman, H. E., Sollas, A. L., Berger, R. E. & Goodman, J. H. Electrophysiological evidence of monosynaptic excitatory transmission between granule cells after seizure-induced mossy fiber sprouting. *J. Neurophysiol.* **90**, 2536–2547 (2003).

16. Engel J., J. Mesial temporal lobe epilepsy: What have we learned? *Neuroscientist* **7**, 340–352 (2001).

17. Dericioglu, N. *et al.* Cell death and survival mechanisms are concomitantly active in the hippocampus of patients with mesial temporal sclerosis. *Neuroscience* **237**, 56–65 (2013).

18. Carter, D. S., Deshpande, L. S., Rafiq, A., Sombati, S. & Delorenzo, R. J. Characterization of spontaneous recurrent epileptiform discharges in hippocampal-entorhinal cortical slices prepared from chronic epileptic animals. *Seizure* **20**, 218–224 (2011).

19. Rubio, C. *et al.* In Vivo Experimental Models of Epilepsy. *Cent. Nerv. Syst. Agents Med. Chem.* **10**, 298–309 (2012).

20. Löscher, W. Animal models of epilepsy for the development of antiepileptogenic and disease-modifying drugs. A comparison of the pharmacology of kindling and post-status epilepticus models of temporal lobe epilepsy. in *Epilepsy Research* vol. 50 105–123 (2002).

21. Kandratavicius, L. *et al.* Animal models of epilepsy: Use and limitations. *Neuropsychiatr. Dis. Treat.* **10**, 1693–1705 (2014).

22. Stoppini, L., Buchs, P. A. & Muller, D. A simple method for organotypic cultures of nervous tissue. *J. Neurosci. Methods* **37**, 173–182 (1991).

23. Heinemann, U., Kann, O. & Schuchmann, S. An Overview of In Vitro Seizure Models in Acute and Organotypic Slices. *Model. Seizures Epilepsy* 35–44 (2006) doi:10.1016/B978-012088554-1/50006-2.

24. Gähwiler, B. H. Organotypic monolayer cultures of nervous tissue. *J. Neurosci. Methods* **4**, 329–342 (1981).

25. Gähwiler, B. H., Capogna, M., Debanne, D., McKinney, R. A. & Thompson, S. M. Organotypic slice cultures: A technique has come of age. *Trends Neurosci.* **20**, 471–477 (1997).

26. Ghoumari, A. M. *et al.* Mifepristone (RU486) protects Purkinje cells from cell death in organotypic slice cultures of postnatal rat and mouse cerebellum. *Proc. Natl. Acad. Sci.* **100**, 7953–7958 (2003).

27. Oishi, Y., Baratta, J., Robertson, R. T. & Steward, O. Assessment of Factors Regulating Axon Growth between the Cortex and Spinal Cord in Organotypic Co-Cultures: Effects of Age and Neurotrophic Factors. *J. Neurotrauma* **21**, 339–356 (2004).

28. Østergaard, K., Finsen, B. & Zimmer, J. Organotypic slice cultures of the rat striatum: an immunocytochemical, histochemical and in situ hybridization study of somatostatin, neuropeptide Y, nicotinamide adenine dinucleotide phosphate-diaphorase, and enkephalin. *Exp. Brain Res.* **103**, 70–84 (1995).

29. Becq, H., Bosler, O., Geffard, M., Enjalbert, A. & Herman, J. P. Anatomical and functional

reconstruction of the nigrostriatal system in vitro: Selective innervation of the striatum by dopaminergic neurons. *J. Neurosci. Res.* **58**, 553–566 (1999).

30. De Simoni, A. & Yu, L. M. Y. Preparation of organotypic hippocampal slice cultures: Interface method. *Nat. Protoc.* **1**, 1439–1445 (2006).

31. Franck, J. E., Pokorny, J., Kunkel, D. D. & Schwartzkroin, P. A. Erratum: Physiologic and morphologic characteristics of granule cell circuitry in human epileptic hippocampus (Epilepsia (1995) 36 (543-558)). *Epilepsia* **36**, 1064 (1995).

32. Dyhrfjeld-Johnsen, J., Berdichevsky, Y., Swiercz, W., Sabolek, H. & Staley, K. J. Interictal Spikes Precede Ictal Discharges in an Organotypic Hippocampal Slice Culture Model of Epileptogenesis. *J. Clin. Neurophysiol.* **27**, 418–424 (2010).

33. Dudek, F. E. & Sutula, T. P. Epileptogenesis in the dentate gyrus: a critical perspective. *Prog. Brain Res.* **163**, 755–773 (2007).

34. Noraberg, J., Kristensen, B. W. & Zimmer, J. Markers for neuronal degeneration in organotypic slice cultures. *Brain Res. Protoc.* **3**, 278–290 (1999).

35. Laake, J. H., Haug, F. M., Wieloch, T. & Ottersen, O. P. A simple in vitro model of ischemia based on hippocampal slice cultures and propidium iodide fluorescence. *Brain Res. Protoc.* **4**, 173–184 (1999).

36. Vismer, M. S., Forcelli, P. A., Skopin, M. D., Gale, K. & Koubeissi, M. Z. The piriform , perirhinal , and entorhinal cortex in seizure generation. **9**, 1–14 (2015).

37. Magalhães, D. M. *et al.* Ex vivo model of epilepsy in organotypic slices-a new tool for drug screening. *J. Neuroinflammation* **15**, 1–18 (2018).

38. Valente, C. A., Meda, F. J., Carvalho, M. & Sebastião, A. M. A Model of Epileptogenesis in Rhinal Cortex- Hippocampus Organotypic Slice Cultures. 1–19 (2020) doi:10.3791/61330.

39. Prinz, M. & Priller, J. The role of peripheral immune cells in the CNS in steady state and disease. *Nat. Neurosci.* **20**, 136–144 (2017).

40. Jeong, H.-K., Ji, K., Min, K. & Joe, E.-H. Brain Inflammation and Microglia: Facts and Misconceptions. *Exp. Neurobiol.* **22**, 59–67 (2013).

41. Lénárt, N., Brough, D. & Dénes, Á. Inflammasomes link vascular disease with neuroinflammation and brain disorders. *J. Cereb. Blood Flow Metab.* **36**, 1668–1685 (2016).

42. Xu, D., Miller, S. D. & Koh, S. Immune mechanisms in epileptogenesis. *Front. Cell. Neurosci.* **7**, 1–8 (2013).

43. Shimada, T., Takemiya, T., Sugiura, H. & Yamagata, K. Role of inflammatory mediators in the pathogenesis of epilepsy. *Mediators Inflamm.* **2014**, (2014).

44. Annamaria Vezzani. Epilepsy and Inflammation in the Brain. *Epilepsy Curr.* **14**, 3–7 (2014).

45. Lobo-Silva, D., Carriche, G. M., Castro, A. G., Roque, S. & Saraiva, M. Balancing the immune response in the brain: IL-10 and its regulation. *J. Neuroinflammation* **13**, 1–10 (2016).

46. Utsuyama, M. & Hirokawa, K. Differential expression of various cytokine receptors in the brain after stimulation with LPS in young and old mice. *Exp. Gerontol.* **37**, 411–420 (2002).

47. Khairova, R. A., Machado-Vieira, R., Du, J. & Manji, H. K. A potential role for pro-inflammatory cytokines in regulating synaptic plasticity in major depressive disorder. *Int. J. Neuropsychopharmacol.* **12**, 561 (2009).

48. Vezzani, A., Balosso, S. & Ravizza, T. The role of cytokines in the pathophysiology of epilepsy. *Brain. Behav. Immun.* **22**, 797–803 (2008).

49. Vezzani, A. *et al.* Functional role of inflammatory cytokines and antiinflammatory molecules in seizures and epileptogenesis. *Epilepsia* **43**, 30–35 (2002).

50. Srinivasan, D., Yen, J. H., Joseph, D. J. & Friedman, W. Cell type-specific interleukin-1β signaling in the CNS. *J. Neurosci.* **24**, 6482–6488 (2004).

51. Martinon, F., Burns, K. & Tschopp, J. The Inflammasome: A molecular platform triggering activation of inflammatory caspases and processing of proIL-β. *Mol. Cell* **10**, 417–426 (2002).

52. Vezzani, A., French, J., Bartfai, T. & Baram, T. Z. The role of inflammation in epilepsy. *Nat. Rev. Neurol.* **7**, 31–40 (2011).

53. Dubé, C., Vezzani, A., Behrens, M., Bartfai, T. & Baram, T. Z. Interleukin-1β contributes to the generation of experimental febrile seizures. *Ann. Neurol.* **57**, 152–155 (2005).

54. De Simoni, M. G. *et al.* Inflammatory cytokines and related genes are induced in the rat hippocampus by limbic status epilepticus. *Eur. J. Neurosci.* **12**, 2623–2633 (2000).

55. Vezzani, A. & Baram, T. Z. New Roles for Interleukin-1 Beta in the Mechanisms of Epilepsy. *Epilepsy Curr.* **7**, 45–50 (2007).

56. Martinon, F., Mayor, A. & Tschopp, J. The inflammasomes: Guardians of the body. *Annu. Rev. Immunol.* **27**, 229–265 (2009).

57. Zhao, G. & Xie, Z. Pyroptosis and neurological diseases. *Neuroimmunol. Neuroinflammation* **1**, 60 (2014).

58. Medzhitov, R. Origin and physiological roles of inflammation. *Nature* **454**, 428–435 (2008).

59. Freeman, L. *et al.* NLR members NLRC4 and NLRP3 mediate sterile inflammasome activation in microglia and astrocytes. *J. Exp. Med.* **214**, 1351–1370 (2017).

60. Edye, M. E., Walker, L. E., Sills, G. J., Allan, S. M. & Brough, D. Epilepsy and the inflammasome: Targeting inflammation as a novel therapeutic strategy for seizure disorders. *Inflammasome* **1**, 36–43 (2014).

61. Sušjan, P., Roškar, S. & Hafner-Bratkovič, I. The mechanism of NLRP3 inflammasome initiation: Trimerization but not dimerization of the NLRP3 pyrin domain induces robust activation of IL-1β. *Biochem. Biophys. Res. Commun.* **483**, 823–828 (2017).

62. Schroder, K. & Tschopp, J. The Inflammasomes. *Cell* **140**, 821–832 (2010).

63. Lampron, A., ElAli, A. & Rivest, S. Innate Immunity in the CNS: Redefining the relationship between the CNS and its Environment. *Neuron* **78**, 214–232 (2013).

64. Singhal, G., Jaehne, E. J., Corrigan, F., Toben, C. & Baune, B. T. Inflammasomes in neuroinflammation and changes in brain function: A focused review. *Front. Neurosci.* **8**, 1–22 (2014).

65. Ting, J. P. Y. *et al.* The NLR Gene Family: A Standard Nomenclature. *Immunity* **28**, 285–287 (2008).

66. Prossomariti, A., Sokol, H. & Ricciardiello, L. Nucleotide-binding domain leucine-rich repeat containing proteins and intestinal microbiota: Pivotal players in colitis and colitis-associated cancer development. *Front. Immunol.* **9**, 1–7 (2018).

67. Franchi, L., Warner, N., Viani, K. & Nuñez, G. Function of Nod-like receptors in microbial recognition and host defense. *Immunol. Rev.* **227**, 106–128 (2009).

68. Stutz, A., Golenbock, D. T. & Latz, E. Inflammasomes: Too big to miss. *J. Clin. Invest.* **119**, 3502–3511 (2009).

69. Kelley, N., Jeltema, D., Duan, Y. & He, Y. The NLRP3 inflammasome: An overview of mechanisms of activation and regulation. *Int. J. Mol. Sci.* **20**, 1–24 (2019).

70. Doyle, S., Ozaki, E. & Campbell, M. Targeting the NLRP3 inflammasome in chronic inflammatory diseases: current perspectives. *J. Inflamm. Res.* **17**, 15 (2015).

71. Song, L., Pei, L., Yao, S., Wu, Y. & Shang, Y. NLRP3 inflammasome in neurological diseases, from functions to therapies. *Front. Cell. Neurosci.* **11**, 1–17 (2017).

72. Walsh, J. G., Muruve, D. A. & Power, C. Inflammasomes in the CNS. *Nat. Rev. Neurosci.* **15**, 84–97 (2014).

73. Gustin, A. *et al.* NLRP3 inflammasome is expressed and functional in mouse brain microglia but not in

astrocytes. *PLoS One* **10**, 1–19 (2015).

74. Maturana, C. J., Aguirre, A. & Sáez, J. C. High glucocorticoid levels during gestation activate the inflammasome in hippocampal oligodendrocytes of the offspring. *Dev. Neurobiol.* **77**, 625–642 (2017).

75. Johann, S. *et al.* NLRP3 inflammasome is expressed by astrocytes in the SOD1 mouse model of ALS and in human sporadic ALS patients. *Glia* **63**, 2260–2273 (2015).

76. Zendedel, A. *et al.* Activation and Regulation of NLRP3 Inflammasome by Intrathecal Application of SDF-1a in a Spinal Cord Injury Model. *Mol. Neurobiol.* **53**, 3063–3075 (2016).

77. Debye, B. *et al.* Neurodegeneration and NLRP3 inflammasome expression in the anterior thalamus of SOD1(G93A) ALS mice. *Brain Pathol.* **28**, 14–27 (2018).

78. Place, D. E. & Kanneganti, T.-D. Recent advances in inflammasome biology. *Curr. Opin. Immunol.* **50**, 32–38 (2018).

79. He, Y., Hara, H. & Núñez, G. Mechanism and Regulation of NLRP3 Inflammasome Activation. *Trends Biochem. Sci.* **41**, 1012–1021 (2016).

80. Di, A. *et al.* The TWIK2 Potassium Efflux Channel in Macrophages Mediates NLRP3 Inflammasome-Induced Inflammation. *Immunity* **49**, 56-65.e4 (2018).

81. Muñoz-Planillo, R. *et al.* K+ Efflux Is the Common Trigger of NLRP3 Inflammasome Activation by Bacterial Toxins and Particulate Matter. *Immunity* **38**, 1142–1153 (2013).

82. Pétrilli, V. *et al.* Activation of the NALP3 inflammasome is triggered by low intracellular potassium concentration. *Cell Death Differ.* **14**, 1583–1589 (2007).

83. Shi, H. *et al.* NLRP3 activation and mitosis are mutually exclusive events coordinated by NEK7, a new inflammasome component. *Nat. Immunol.* **17**, 250–258 (2016).

84. Schmid-Burgk, J. L. *et al.* A genome-wide CRISPR (clustered regularly interspaced short palindromic repeats) screen identifies NEK7 as an essential component of NLRP3 inflammasome activation. *J. Biol. Chem.* **291**, 103–109 (2016).

85. Lu, A. *et al.* dependent Inflammasomes. *Cell* **156**, 1193–1206 (2014).

86. Kayagaki, N. *et al.* Non-canonical inflammasome activation targets caspase-11. *Nature* **479**, 117–121 (2011).

87. Kayagaki, N. *et al.* Noncanonical Inflammasome Activation by Intracellular LPS Independent of TLR4. *Science (80-.).* **341**, 1246–1249 (2013).

88. Hagar, J. A., Powell, D. A., Aachoui, Y., Ernst, R. K. & Miao, E. A. Cytoplasmic LPS activates caspase-11: Implications in TLR4-independent endotoxic shock. *Science (80-.).* **341**, 1250–1253 (2013).

89. Niikura, T., Tajima, H. & Kita, Y. Neuronal Cell Death in Alzheimers Disease and a Neuroprotective Factor, Humanin. *Curr. Neuropharmacol.* **4**, 139–147 (2006).

90. Engel, T. & Henshall, D. C. Apoptosis, Bcl-2 family proteins and caspases: The ABCs of seizure-damage and epileptogenesis? *Int. J. Physiol. Pathophysiol. Pharmacol.* **1**, 97–115 (2009).

91. Dingledine, R., Varvel, N. H. & Dudek, F. E. When and How Do Seizures Kill Neurons, and Is Cell Death Relevant to Epileptogenesis? in *Physiology & behavior* vol. 176 109–122 (2014).

92. Lorigados, L. *et al.* Excitotoxicity and neuronal death in epilepsy. *Biotecnol. Apl.* **30**, 1–8 (2013).

93. Fujikawa, D. G. Prolonged seizures and cellular injury: Understanding the connection. *Epilepsy Behav.* **7**, 3–11 (2005).

94. Bengzon, J., Mohapel, P., Ekdahl, C. T. & Lindvall, O. Neuronal apoptosis after brief and prolonged seizures. *Prog. Brain Res.* **135**, 111–119 (2002).

95. Scaffidi, P., Misteli, T. & Bianchi, M. E. Release of chromatin protein HMGB1 by necrotic cells triggers inflammation. *Nature* **418**, 191–195 (2002).

96. Mariathasan, S. *et al.* Differential activation of the inflammasome by caspase-1 adaptors ASC and Ipaf. *Nature* **430**, 213–218 (2004).

97. Sansonetti, P. J. *et al.* Caspase-1 activation of IL-1β and IL-18 are essential for Shigella flexneri-induced inflammation. *Immunity* **12**, 581–590 (2000).

98. Ma, Y. *et al.* Research progress of the relationship between pyroptosis and disease. **10**, 2213–2219 (2018).

99. Li, P. *et al.* Mice deficient in IL-1β-converting enzyme are defective in production of mature IL-1β and resistant to endotoxic shock. *Cell* **80**, 401–411 (1995).

100. Monack, D. M., Detweiler, C. S. & Falkow, S. Salmonella pathogenicity island 2-dependent macrophage death is mediated in part by the host cysteine protease caspase-1. *Cell. Microbiol.* **3**, 825–837 (2001).

101. Fink, S. L. & Cookson, B. T. Apoptosis, pyroptosis, and necrosis: Mechanistic description of dead and dying eukaryotic cells. *Infect. Immun.* **73**, 1907–1916 (2005).

102. Shi, J., Gao, W. & Shao, F. Pyroptosis : Gasdermin- Mediated Programmed Necrotic Cell Death. *Trends Biochem. Sci.* **xx**, 1–10 (2016).

103. Wang, K. *et al.* Structural Mechanism for GSDMD Targeting by Autoprocessed Caspases in Pyroptosis. *Cell* **180**, 941-955.e20 (2020).

104. Liu, X. *et al.* Inflammasome-activated gasdermin D causes pyroptosis by forming membrane pores. *Nature* **535**, 153–158 (2016).

105. Kayagaki, N. *et al.* IRF2 transcriptionally induces GSDMD expression for pyroptosis. *Sci. Signal.* **12**, (2019).

106. Tan, M. S. *et al.* Amyloid-β induces NLRP1-dependent neuronal pyroptosis in models of Alzheimer's disease. *Cell Death Dis.* **5**, 1–12 (2014).

107. Kim, J. Y., Paton, J. C., Briles, D. E., Rhee, D. K. & Pyo, S. Streptococcus pneumoniae induces pyroptosis through the regulation of autophagy in murine microglia. *Oncotarget* **6**, 44161–44178 (2015).

108. Fu, Q. *et al.* NLRP3/Caspase-1 Pathway-Induced Pyroptosis Mediated Cognitive Deficits in a Mouse Model of Sepsis-Associated Encephalopathy. *Inflammation* **42**, 306–318 (2019).

109. Wang, S., Yuan, Y. H., Chen, N. H. & Wang, H. B. The mechanisms of NLRP3 inflammasome/pyroptosis activation and their role in Parkinson's disease. *Int. Immunopharmacol.* **67**, 458–464 (2019).

110. Coll, R. C. *et al.* Potential Therapeutic for Inflammatory Diseases. *Nat. Med.* **21**, 248–255 (2015).

111. Youm, Y.-H. *et al.* Ketone body β-hydroxybutyrate blocks the NLRP3 inflammasome-mediated inflammatory disease HHS Public Access. *Nat Med* **21**, 263–269 (2015).

112. Tan, C. C. *et al.* NLRP1 inflammasome is activated in patients with medial temporal lobe epilepsy and contributes to neuronal pyroptosis in amygdala kindling-induced rat model. *J. Neuroinflammation* **12**, 1–12 (2015).

113. Ramazi, S. *et al.* Neuroprotective and anticonvulsant effects of sinomenine in kainate rat model of temporal lobe epilepsy: Involvement of oxidative stress, inflammation and pyroptosis. *J. Chem. Neuroanat.* **108**, (2020).

114. Perregaux, D. G. *et al.* Identification and characterization of a novel class of interleukin-1 post-translational processing inhibitors. *J. Pharmacol. Exp. Ther.* **299**, 187–197 (2001).

115. Vitaliti, G., Pavone, P., Mahmood, F., Nunnari, G. & Falsaperla, R. Targeting inflammation as a therapeutic strategy for drug-resistant epilepsies: An update of new immune-modulating approaches. *Hum. Vaccines Immunother.* **10**, 868–875 (2014).

116. Kenney-Jung, D. L. *et al.* Super-refractory status epilepticus and febrile infection-related epilepsy syndrome treated with anakinra. *Ann. Neurol.* **80**, 939–945 (2016).

117. DeSena, A. D., Do, T. & Schulert, G. S. Systemic autoinflammation with intractable epilepsy managed

with interleukin-1 blockade. *J. Neuroinflammation* **15**, 1–6 (2018).

118. Wang, M., Deng, X., Xie, Y. & Chen, Y. Astaxanthin attenuates neuroinflammation in status epilepticus rats by regulating the atp-p2x7r signal. *Drug Des. Devel. Ther.* **14**, 1651–1662 (2020).

119. Vezzani, A. *et al.* Powerful anticonvulsant action of IL-1 receptor antagonist on intracerebral injection and astrocytic overexpression in mice. *Proc. Natl. Acad. Sci. U. S. A.* **97**, 11534–11539 (2000).

120. Meng, X. F. *et al.* Inhibition of the NLRP3 inflammasome provides neuroprotection in rats following amygdala kindling-induced status epilepticus. *J. Neuroinflammation* **11**, 1–12 (2014).

121. Zahid, A., Li, B., John, A., Kombe, K. & Jin, T. Pharmacological Inhibitors of the NLRP3 Inflammasome. **10**, 1–10 (2019).

122. Coll, R. C. *et al.* MCC950 directly targets the NLRP3 ATP- hydrolysis motif for inflammasome inhibition. **15**, (2019).

123. Tapia-Abellán, A. *et al.* MCC950 closes the active conformation of NLRP3 to an inactive state. *Nat. Chem. Biol.* **15**, 560–564 (2019).

124. Levy, M., Thaiss, C. A. & Elinav, E. Taming the inflammasome. *Nat. Med.* **21**, 213–215 (2015).

125. Barbarosie, M. & Avoli, M. CA3-driven hippocampal-entorhinal loop controls rather than sustains in vitro limbic seizures. *J. Neurosci.* **17**, 9308–9314 (1997).

126. Rutecki, P. A. & Yang, Y. Total epileptiform activity in the CA3 region of hippocampal slices produced by philocarpine. *J. Neurophysiol.* **79**, 3019–3029 (1998).

127. Anderson, W. W. & Collingridge, G. L. The LTP Program: A data acquisition program for on-line analysis of long-term potentiation and other synaptic events. *J. Neurosci. Methods* **108**, 71–83 (2001).

128. Berdichevsky, Y., Dzhala, V., Mail, M. & Staley, K. J. Interictal spikes, seizures and ictal cell death are not necessary for post-traumatic epileptogenesis in vitro. *Neurobiol. Dis.* **45**, 774–785 (2012).

129. Lee, S. B. *et al.* Serum deprivation-induced reactive oxygen species production is mediated by Romo1. *Apoptosis* **15**, 204–218 (2010).

130. Hanslick, J. L. *et al.* Dimethyl sulfoxide (DMSO) produces widespread apoptosis in the developing central nervous system. *Neurobiol. Dis.* **34**, 1–10 (2009).

131. Shi, J. *et al.* Cleavage of GSDMD by inflammatory caspases determines pyroptotic cell death. *Nature* **526**, 660–665 (2015).

132. Block, M. L., Zecca, L. & Hong, J. S. Microglia-mediated neurotoxicity: Uncovering the molecular mechanisms. *Nat. Rev. Neurosci.* **8**, 57–69 (2007).

133. Giulian, D., Baker, T. J., Shih, L. C. N. & Lachman, L. B. Interleukin 1 of the central nervous system is produced by ameboid microglia. *J. Exp. Med.* **164**, 594–604 (1986).

134. Treiman, D. M. GABAergic mechanisms in epilepsy. *Epilepsia* **42**, 8–12 (2001).

135. Yan, X.-X. & Jeromin, A. Spectrin Breakdown Products (SBDPs) as Potential Biomarkers for Neurodegenerative Diseases. *Curr. Transl. Geriatr. Exp. Gerontol. Rep.* **1**, 85–93 (2012).

136. Xu, T. *et al.* NADPH oxidase 2-mediated NLRP1 inflammasome activation involves in neuronal senescence in hippocampal neurons in vitro. *Int. Immunopharmacol.* **69**, 60–70 (2019).

137. Baroja-Mazo, A. *et al.* The NLRP3 inflammasome is released as a particulate danger signal that amplifies the inflammatory response. *Nat. Immunol.* **15**, 738–748 (2014).

8. Annexes

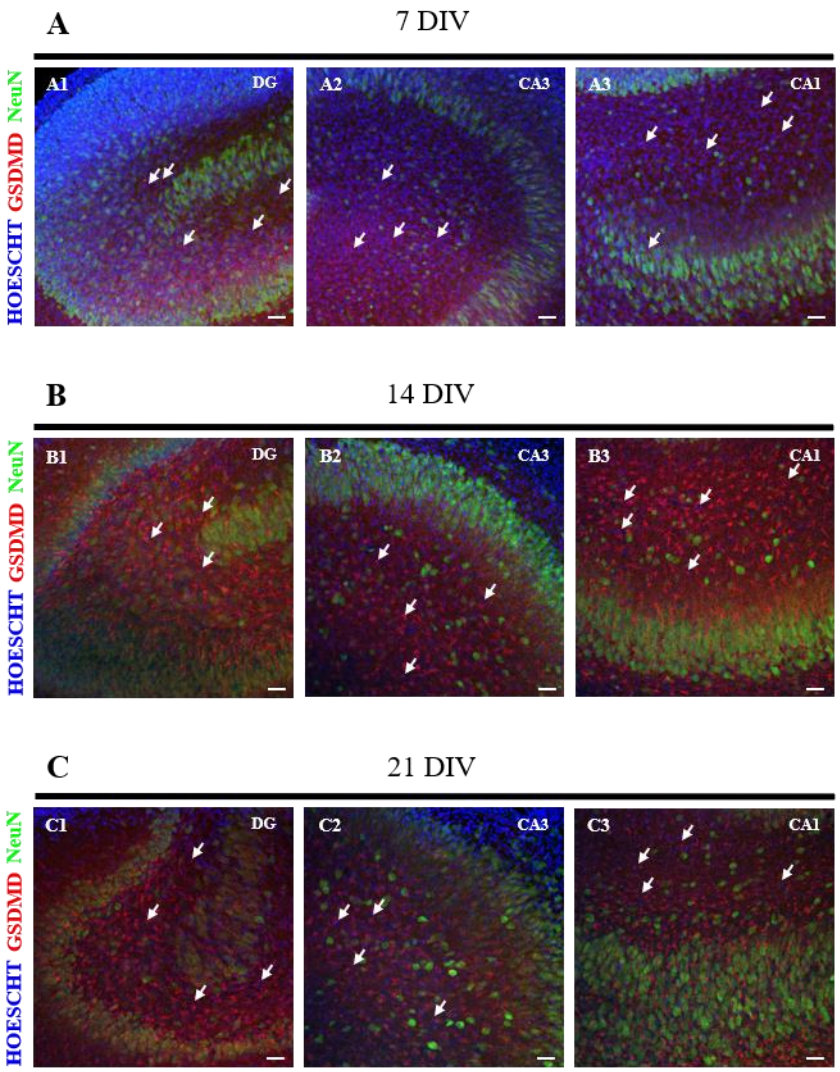

Annex 1: Co-localization of GSDMD with neurons in epileptic-like rhinal cortex-hippocampus organotypic slices. Representative images of NeuN stained neurons (green), GSDMD-stained cells (red) and the nuclear marker HOESCHT (blue) at **(A)** 7 DIV, **(B)** 14 DIV and **(C)** 21 DIV were acquired on a confocal laser microscope (Zeiss LSM 710) with a 20x objective. Arrows point to $NeuN^{-}/GSDMD^{+}$ cells (in orange). Scale-bar, 50 µm.

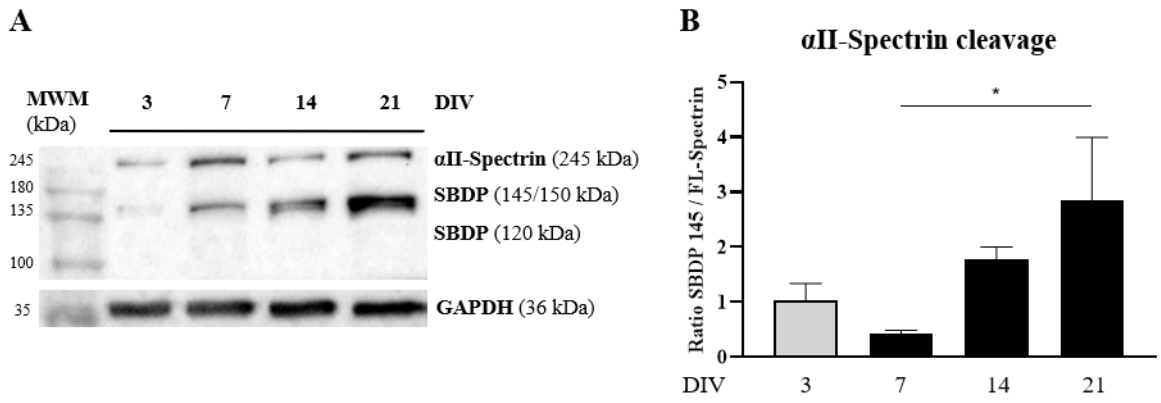

Annex 2: Expression pattern of αII-Spectrin and SBDPs in epileptic-like rhinal cortex-hippocampus organotypic slices. (A) Representative immunoblots of FL-Spectrin (245kDa), SPDPs (145/150 kDa) and GAPDH (36 kDa) at 3, 7, 14 and 21 DIV. **(B)** Densitometry analysis of FL-Spectrin and SBDP 145/150 was performed with ImageJ software. Results are presented as the ratio FL-Spectrin to SBDP 145/150. The presence of SPDP 145/150 kDa indicates αII-Spectrin cleavage by calpains and reveals neuronal death by necrosis. SBDP 120 is not present indicating the absence of neuronal death by apoptosis. All values are presented as mean ± SEM. N= 6-8 independent cultures. *p<0.05, , by one-way ANOVA followed by Tukey's multiple comparison test. Statistical tests were performed according to the connecting lines above the bars. Adapted from Cláudia Cavacas Master Thesis, 2017.

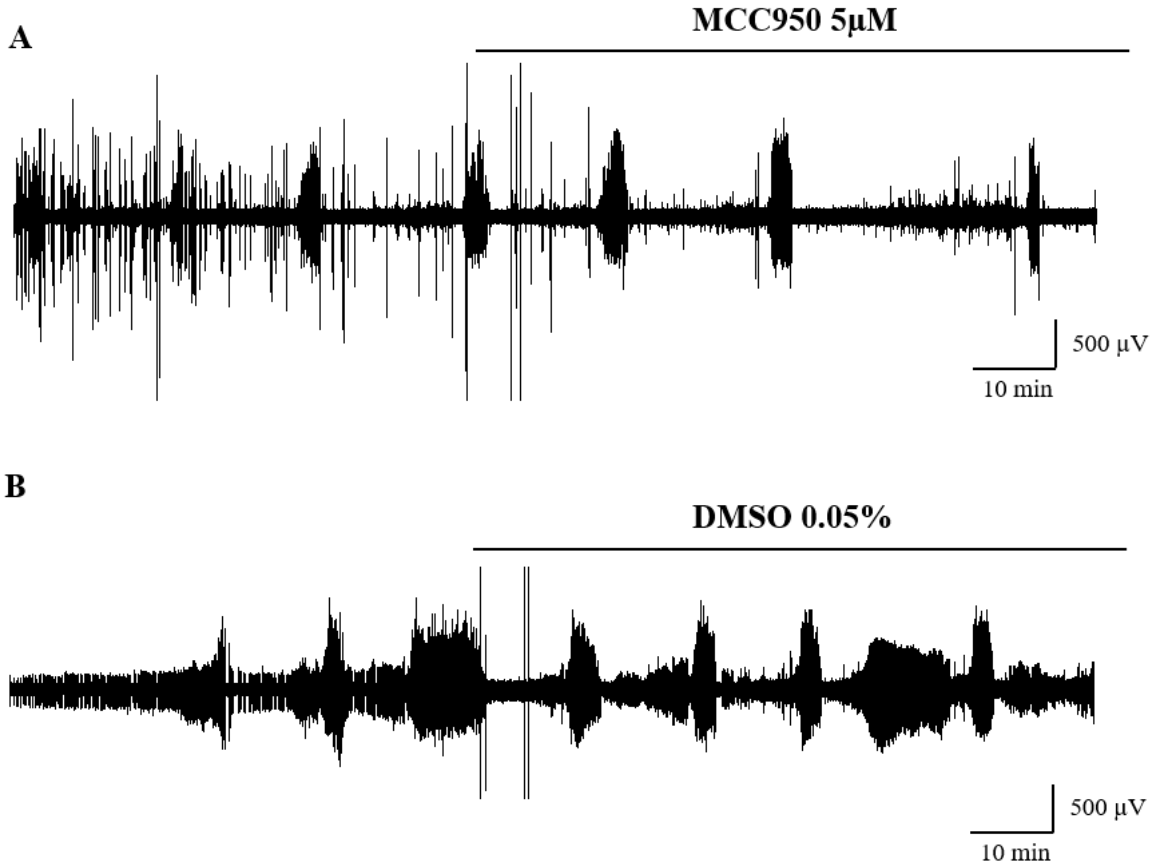

Annex 3: Representative spontaneous epileptiform activity in epileptic-like rhinal cortex-hippocampus organotypic slices recorded at 14 DIV under various conditions. Slices were exposed to **(A)** 5µM MCC950 and **(B)** 0,05% DMSO after 30 min of recording. MCC950 5µM reduces burst recurrence and DMSO alone does not change epileptiform activity.

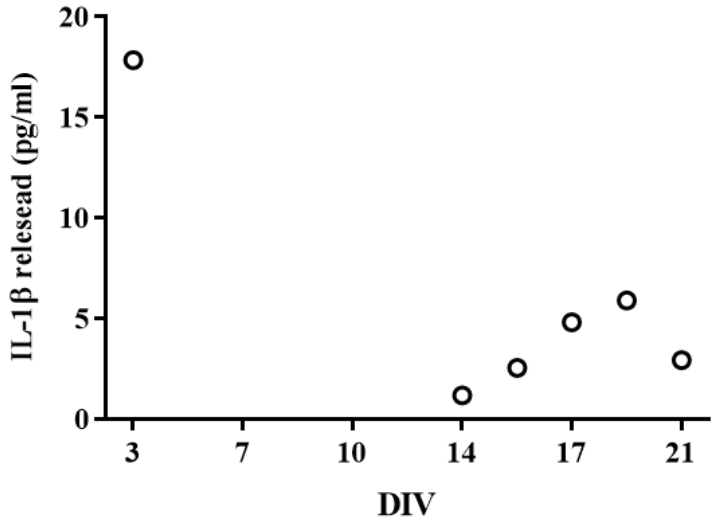

Annex 4: IL-1β released by rhinal cortex-hippocampus organotypic slices kept in the presence of 25% horse serum throughout the whole culture. IL-1β was quantified in culture medium collected at 3, 6, 7, 8, 10, 13, 14, 15, 17, 20 and 21 DIV by ELISA. N=1. Most values were not measurable, indicating a poor IL-1β release in these slices. Quantification was performed in collaboration with Mafalda Carvalho.

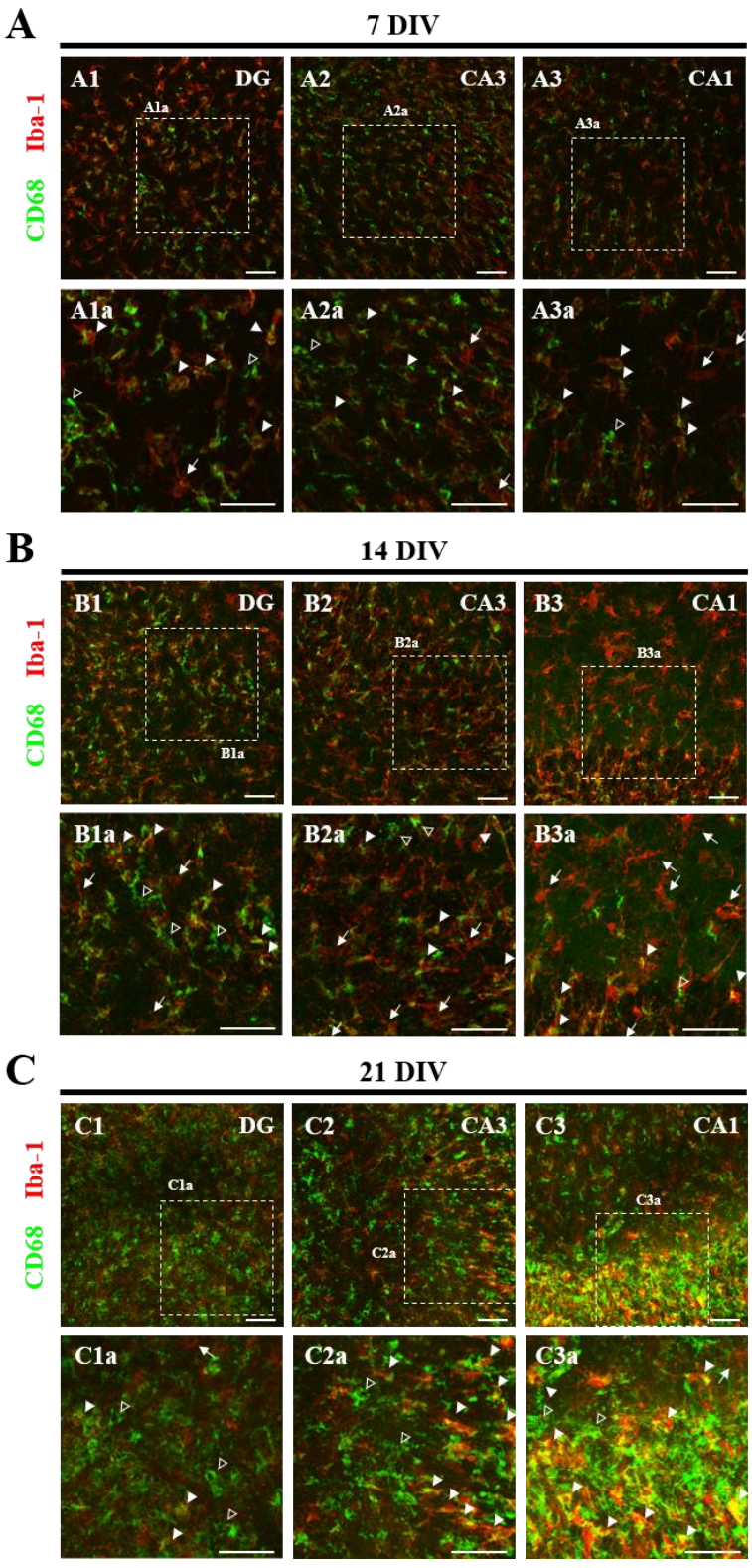

Annex 5: Double staining of Iba-1 and CD68 in epileptic-like rhinal cortex-hippocampus organotypic slices. Representative images of Iba1 (red) and CD68 (green) stained microglia, and the nuclear marker HOESCHT (blue), were acquired at **(A)** 7 DIV, **(B)** 14 DIV and **(C)** 21 DIV, on a confocal laser microscope with a 20x objective. Magnified images of the dashed areas are shown. Arrows point to $Iba1^{+}/CD68^{-}$ resting microglia, arrowheads indicate $Iba1^{+}/CD68^{+}$ bushy/amoeboid M1 microglia and open arrowheads reveal $Iba1^{+}/CD68^{+}$ hyper-ramified microglia, suggestive of M2 microglia. Scale-bar, 50 µm. Courtesy of Mafalda Carvalho.